CHAPTER - III

CHAPTER III

RESULTS OF THE EXPERIMENTATION

3.1 Introduction.

As already mentioned in chapter II the designing, fabrication and testing of the EMC patch antenna were done. Ferrites $MgFe_2O_4$ and $Mg_{0.4}Mn_{0.5}Zn_{0.1}Al_{0.8}Fe_{1.2}O_4$, used as an overlay on the patch antenna were prepared by wet chemical method. In order to confirm the formation of ferrite, some physical properties of these synthesized ferrites were studied as a part of the research work. These studies were undertaken with the sole purpose of confirming the formation of the required ferrite. Therefore the other aspects of the physical properties of the ferrite have not been elaborated in this thesis. The main work consists of the fabrication of the EMC patch antenna using thick film technology and testing these antennas for the effect of feed line positions and ferrite overlay. The results of these along with the values studied are given in this chapter.

3.2 Properties of the synthesized ferrite in pellet form.

$MgFe_2O_4$ and $Mg_{0.4}Mn_{0.5}Zn_{0.1}Al_{0.8}Fe_{1.2}O_4$ ferrites were synthesized as already described in chapter II. In order to ascertain the proper formation of the mixed and single ferrite some of its physical properties were studied. Results of the properties of ferrite are as follows.

3.2.1 X-Ray Diffraction patterns.

The X- Ray diffraction patterns of the powered ferrite samples were recorded with the help of X- Ray diffractometer (Philips, PW-1710) with CuK_α radiation(λ=1.5418A^0) at USIC, S. U. Kolhapur.

The X Ray Diffraction patterns of the present samples are shown in figures 3.1 (a), (b). Both the samples exhibit cubic spinal structure. The absence of

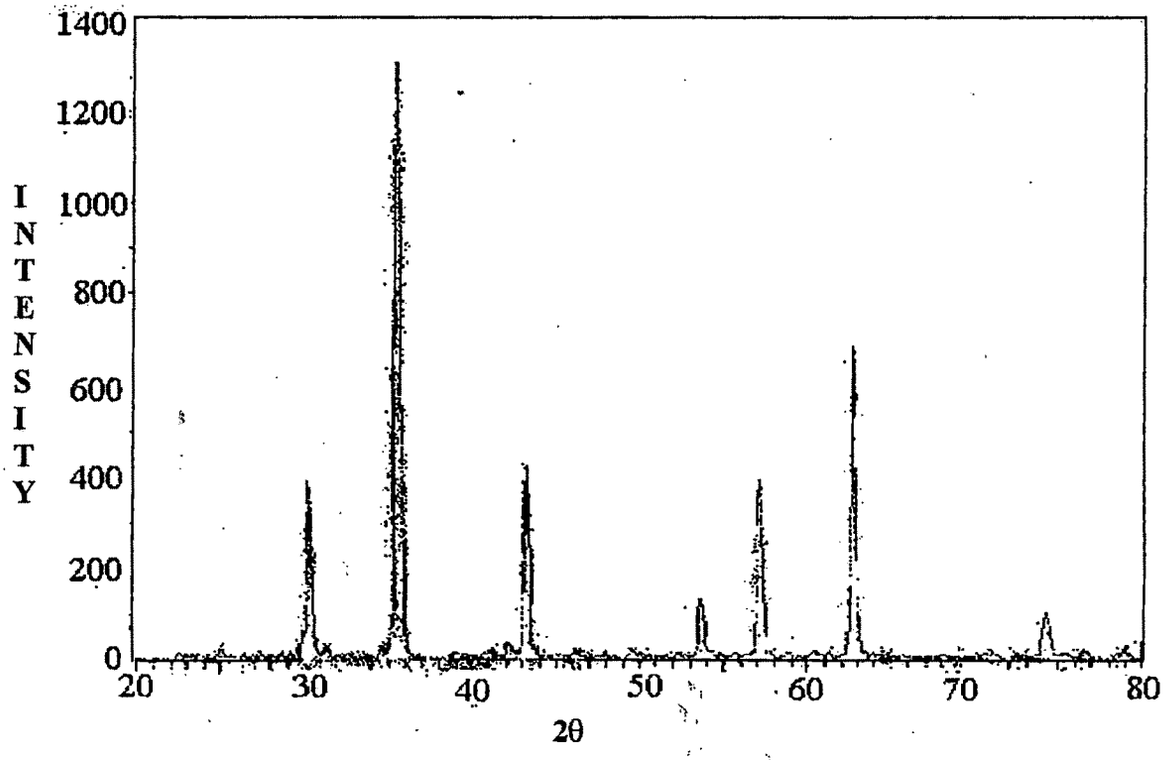

FIGURE 3.1(a) : X-Ray Diffraction Patterns of $MgFe_2O_4$

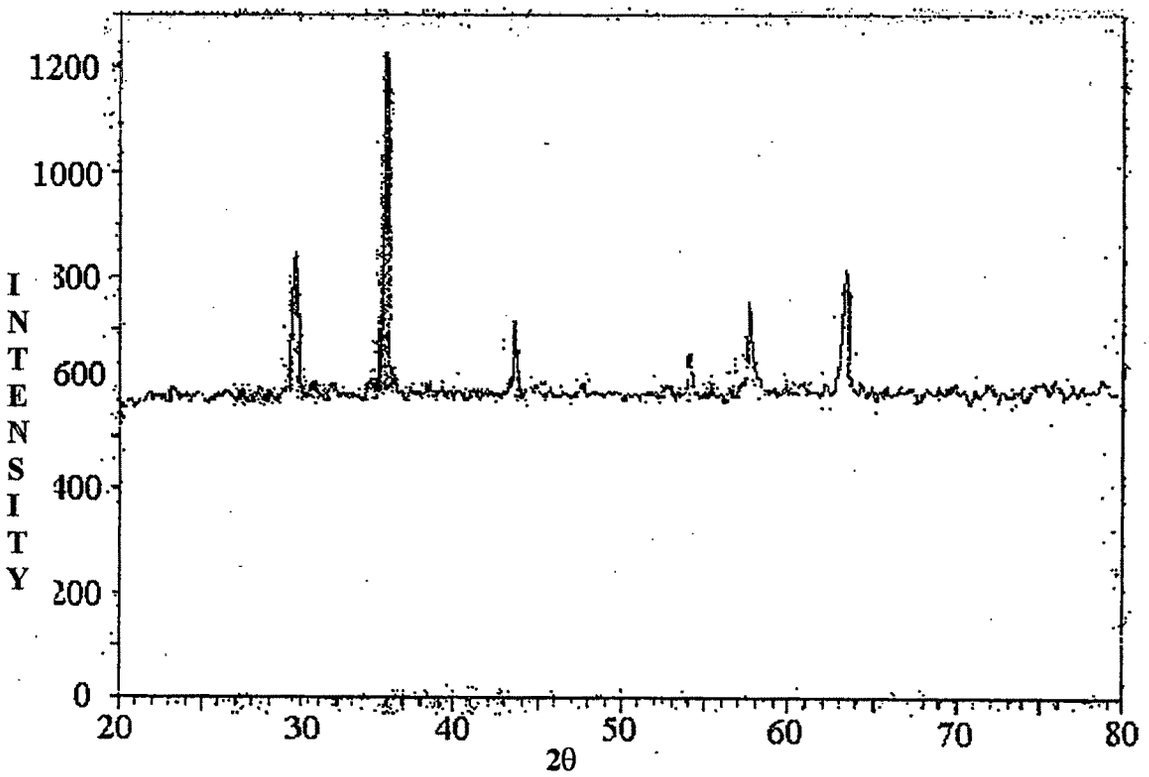

FIGURE 3.1(b) : X-Ray Diffraction Pattern of $Mg_{0.4}Mn_{0.5}Zn_{0.1}Al_{0.8}Fe_{1.2}O_4$

extra line confirms the single-phase formation of ferrite samples. In both XRD patterns, the (311) plane is the most intense one, indicating the spinel structure. For face centered cubic structure, the cyclic sum of miller indices viz. (h+k), (k+l) and (l+h) in an even number. This is observed in the present case for both $MgFe_2O_4$ and $Mg_{0.4}Mn_{0.5}Zn_{0.1}Al_{0.8}Fe_{1.2}O_4$ ferrites. The inter planer relations are calculated using the relation

$$2\,d\sin\theta = n\,\lambda \qquad 3.1$$

Where,

d = inter planer distance

θ =angle of diffraction

n = order of diffraction

λ = 1.5418 A^0 wavelength of the light used.

The lattice parameters (a) are calculated by using the relation

$$a = d_{cal}\sqrt{h^2 + k^2 + l^2} \qquad 3.2$$

The observed and calculated d values are tabulated in table 3.1 (a and b) below.

X ray density is calculated by using following relation.

$$dx = \frac{8\,M}{N\,a^3} \qquad 3.3$$

M = molecular weight of the sample.

N = 6.023 x 10^{23} is the Avagadros number.

a = Lattice parameter calc1ulated from XRD.

$$\text{Porosity} = \frac{dx - da}{dx} \times 100 \qquad 3.4$$

da = actual density.

Calculated porosity for both the samples is tabulated in table 3.2 along with its partial size.

Table 3.1 : The XRD data of $MgFe_2O_4$ **$a_{avg} = 8.366064$**

Plane	d_{obs} A^0	d_{cal} A^0	a A^0
220	2.9499	2.95162	8.3484
311	2.5167	2.15187	8.3536
400	2.0909	2.0918	8.3673
422	1.7078	1.7092	8.3733
333	1.6099	1.6112	8.3720
440	1.4791	1.4803	8.3736
533	1.2760	1.277	8.3741

Table 3.1 : The XRD data of $Mg_{0.4}Mn_{0.5}Zn_{0.1}Al_{0.8}Fe_{1.2}O_4$ **$a_{avg} = 8.3075$**

Plane	d_{obs} A^0	d_{cal} A^0	a A^0
220	2.9299	2.9322	8.2936
311	2.4997	2.5017	8.2973
400	2.0751	2.0767	8.3069
422	1.6960	1.6973	8.3152
333	1.5988	1.6000	8.3141
440	1.4690	1.4702	8.3165

3.2.2 Infrared Studies

The Infra Red spectra of ferrite samples were recorded on Perkin- Elmer 783 IR spectrometer (USIC, S. U. Kolhapur) Fig 3.2 (a), (b) shows the IR spectra of $MgFe_2O_4$ and $Mg_{0.4}Mn_{0.5}Zn_{0.1}Al_{0.8}Fe_{1.2}O_4$ ferrites respectively.

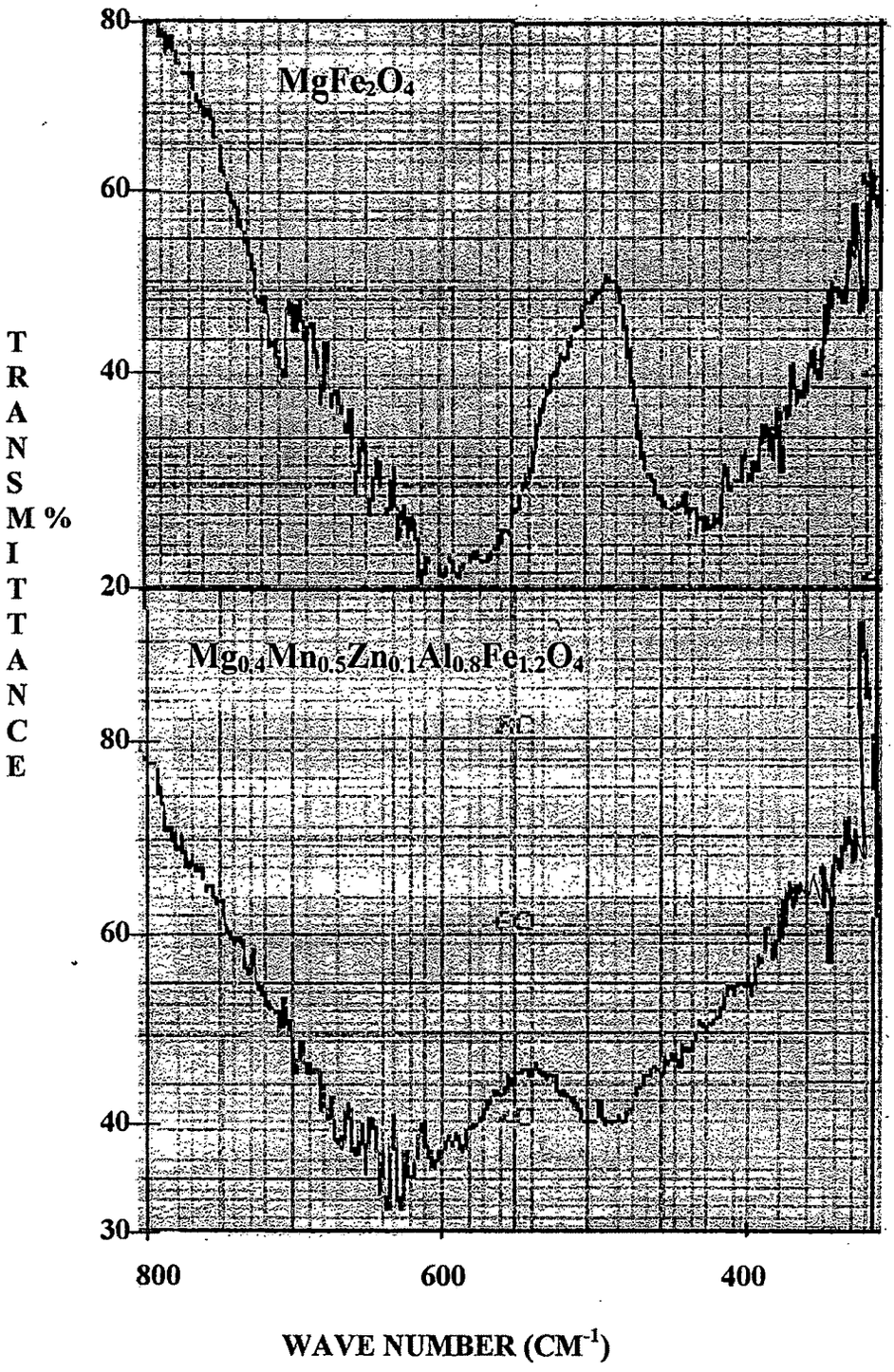

FIGURE 3.2 : Infrared spectrum of the ferrite samples

From the figures it is seen that the synthesized ferrite has two dominant peaks at 600 cm^{-1} and 400 cm^{-1} as is observed for any spinel ferrite of $MgFe_2O_4$ and $Mg_{0.4}Mn_{0.5}Zn_{0.1}Al_{0.8}Fe_{1.2}O_4$.

3.2.3 Scanning Electron Microscope studies.

The morphology of the samples were observed using Scanning Electron microscope (Phillips, Model XL-30). Figure 3.3 (a) and (b) shows micrographs of $MgFe_2O_4$ and $Mg_{0.4}Mn_{0.5}Zn_{0.1}Al_{0.8}Fe_{1.2}O_4$ ferrites respectively.

From the micrographs it is clear that the grains have grown sufficiently indicating the completion of solid-state reaction. The grains in $Mg_{0.4}Mn_{0.5}Zn_{0.1}Al_{0.8}Fe_{1.2}O_4$ ferrite are comparatively larger than those in $MgFe_2O_4$ ferrite. The porosity seems to be more in case of $MgFe_2O_4$ ferrite as compared to $Mg_{0.4}Mn_{0.5}Zn_{0.1}Al_{0.8}Fe_{1.2}O_4$ ferrite. The porosity calculated from XRD supports the above observations.

The average grain was measured by line intercept method, using the magnification bar present on SEM micrographs. The average grain diameters are given in table 3.2 along with the porosity and particle size measured from XRD data.

Table 3.2 Porosity and partical size data

Sample	Porosity %	Particle size (XRD) μm	Particle diameter (SEM) μm
$MgFe_2O_4$	46.24	0.1062	0.200
$Mg_{0.4}Mn_{0.5}Zn_{0.1}Al_{0.8}Fe_{1.2}O_4$	38.5	0.1109	0.250

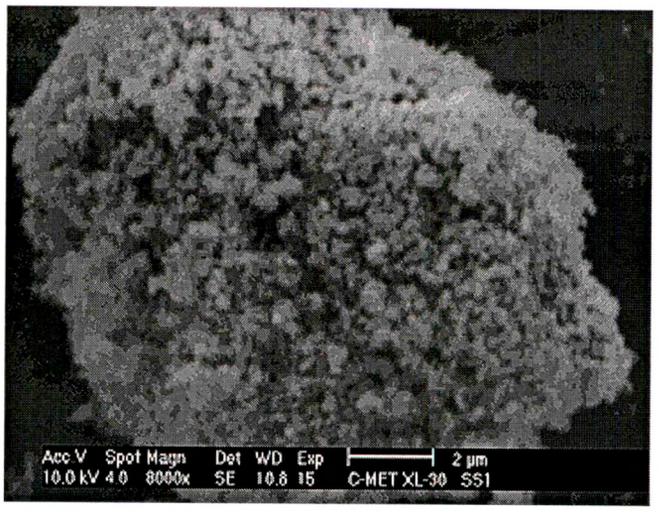

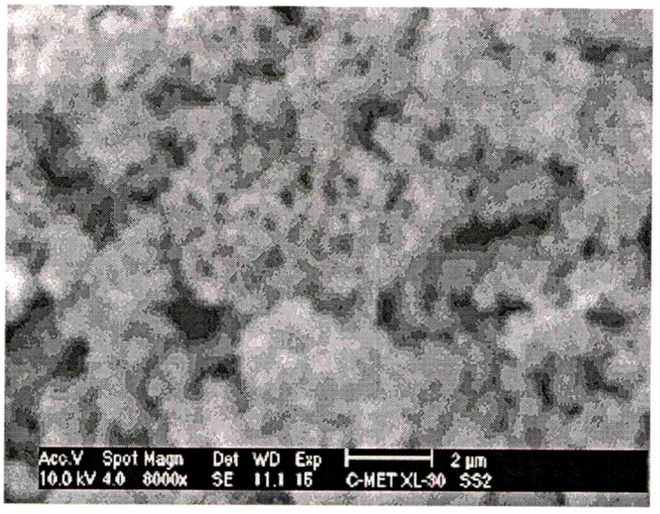

FIGURE 3.3(a,b): SEM micrographs of $MgFe_2O_4$ (S1) and $Mg_{0.4}Mn_{0.5}Zn_{0.1}Al_{0.8}Fe_{1.2}O_4$ (S2) ferrites respectively.

It is observed that grain size is high for $Mg_{0.4}Mn_{0.5}Zn_{0.1}Al_{0.8}Fe_{1.2}O_4$ than $MgFe_2O_4$. The porosity variation supports the above observation by showing an opposite trend. The porosity in case of single ferrite is more. The mixed ferrite seems to be denser with large grain size. The grain growths depends upon the several factors such as particle size of initial ingredient, their distribution, and particle shape, inter-particle porosity, homogeneity in chemical composition and activated sintering etc [85].

3.2.4 Energy Dispersion Analysis of X-rays (EDAX)

EDAX is a technique for quantitative analysis of the sample. It gives atomic weight percentage ratio. Expected and obtained atomic weight ratios are given below.

Table 3.3 EDAX data

	Mg:Fe:O	**Mg:Mn:Zn:Al:Fe:O**
Expected	**1 : 2 : 4**	**0.4 : 0.5 : 0.1 : 0.8 : 1.2 : 4**
Obtained	**1 : 2.5 : 3.6**	**0.4 : 0.5 : 0.1 : 0.7 : 1.4 : 3.5**

These calculations have been made with respect to content of Mg. From the data it is seen that there is a slight increase in Fe content and decrease in O content in the sample prepared. The EDAX plots are shown in Figures 3.4 (a) and (b) for $MgFe_2O_4$ and $Mg_{0.4}Mn_{0.5}Zn_{0.1}Al_{0.8}Fe_{1.2}O_4$ respectively.

C:\UNIV\ss1.spc

Label:

kV:10.0 Tilt:0.0 Take-off:35.0 Det Type:SUTW+ Res:134 Tc:50

FS : 3904 Lsec : 85 30-Aug- 1 17:27:41

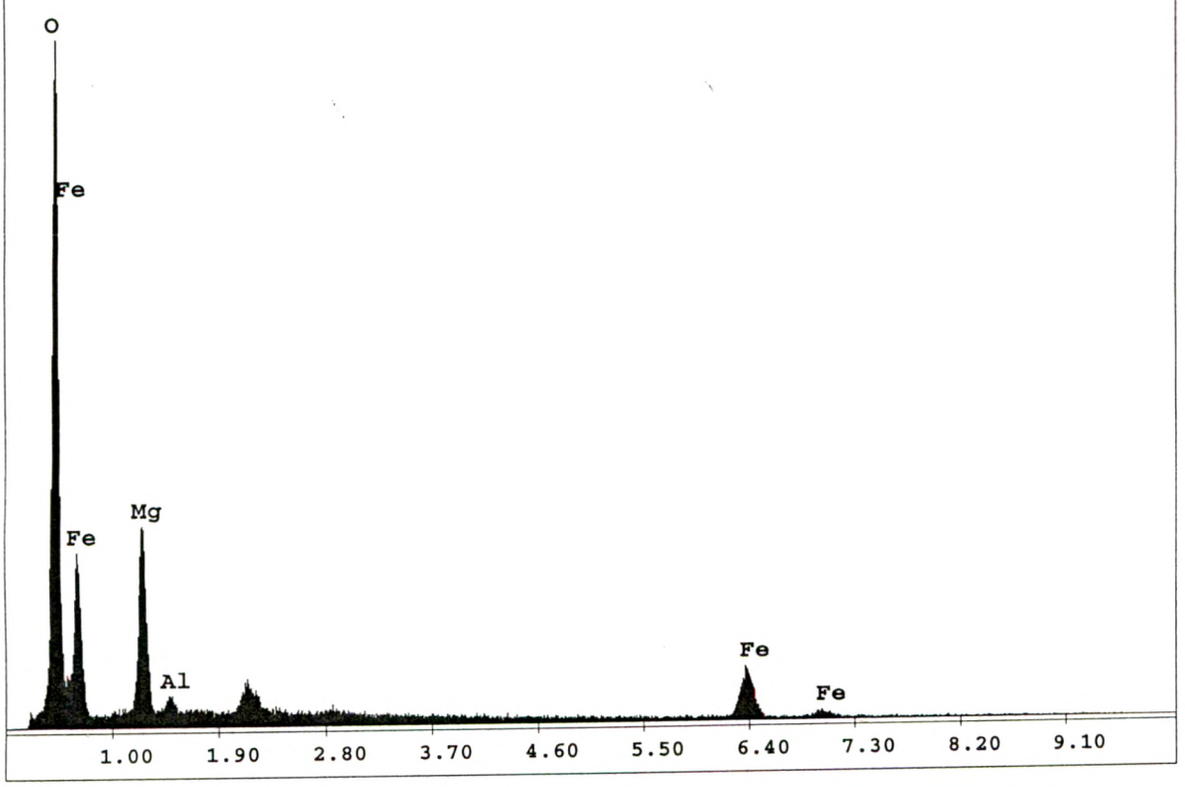

EDAX ZAF Quantification (Standardless)
Element Normalized

Element	Wt %	At %	K-Ratio	Z	A	F
O K	25.56	49.88	0.2087	1.1268	0.7231	1.0021
MgK	10.85	13.93	0.0702	1.0800	0.5994	1.0001
AlK	1.06	1.23	0.0075	1.0412	0.6798	1.0001
FeK	62.53	34.96	0.5726	0.9147	1.0011	1.0000
Total	100.00	100.00				

Element	Net Inte.	Bkgd Inte.	Inte. Error	P/B
O K	235.72	2.31	0.71	102.23
MgK	78.01	7.13	1.28	10.94
AlK	7.71	8.51	5.67	0.91
FeK	31.63	1.64	1.98	19.35

FIGURE 3.4<a>: EDAX report of $MgFe_2O_4$.

C:\UNIV\ss2.spc

Label:

kV:10.0 Tilt:0.0 Take-off:35.0 Det Type:SUTW+ Res:134 Tc:50

FS : 8844 Lsec : 156 30-Aug- 1 17:32:42

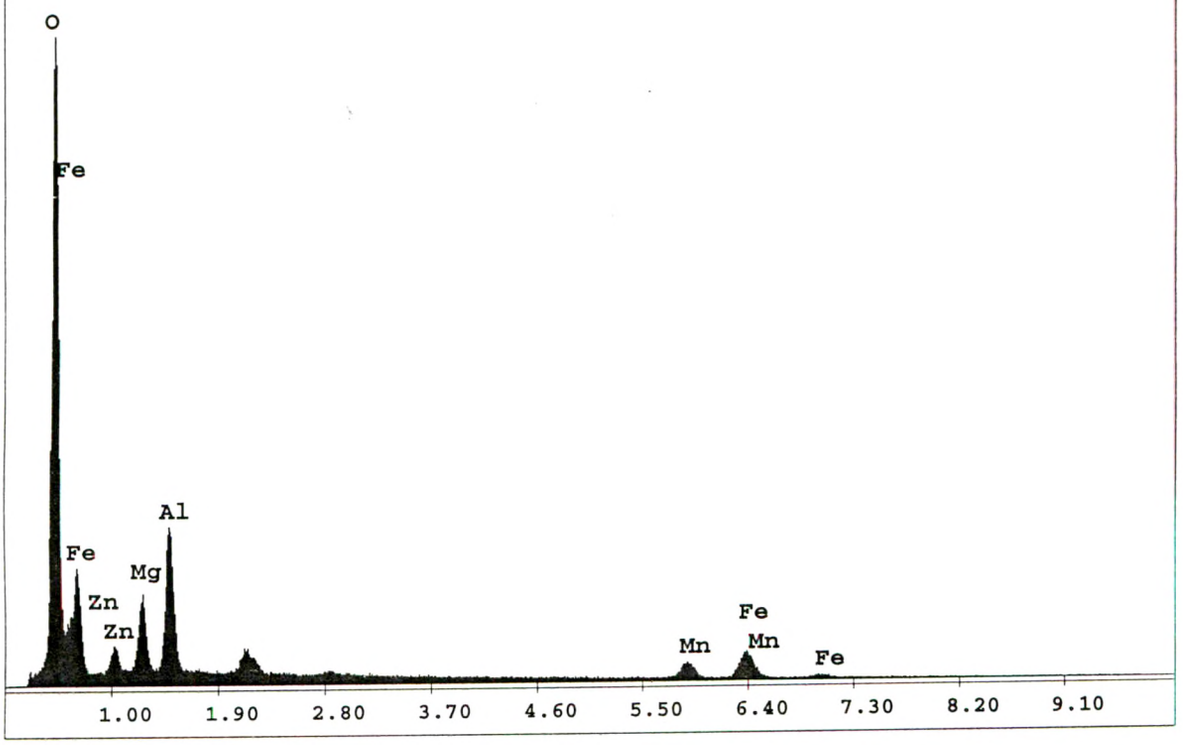

EDAX ZAF Quantification (Standardless)
Element Normalized

Element	Wt %	At %	K-Ratio	Z	A	F
O K	28.08	52.69	0.2260	1.1244	0.7147	1.0016
ZnL	3.52	1.62	0.0170	0.8940	0.5383	1.0007
MgK	4.76	5.88	0.0315	1.0766	0.6133	1.0011
AlK	9.53	10.61	0.0706	1.0383	0.7127	1.0001
MnK	15.45	8.44	0.1389	0.8985	1.0005	1.0001
FeK	38.65	20.77	0.3526	0.9113	1.0011	1.0002
Total	100.00	100.00				

Figure 3.4 <b> : EDAX report of $Mg_{0.4}Mn_{0.5}Zn_{0.1}Al_{0.8}Fe_{1.2}O_4$.

3.2.5 Saturation magnetization

The magnetization measurements were made by using a high field hysterisis loop tracer at S. U. Kolhapur (designed by T.I.F.R, Mumbai). Measurements of saturation magnetization for each sample were carried out directly from the trace on the CRO screen. The screen was properly illuminated and calibrated. The standard Ni sample with saturation magnetization of 53.34 emu/gm and mass of 0.6922 gm was introduced into balancing coil and current was gradually increased until the hysterisis loop on CRO screen saturates.

As an example the photograph of hysterisis loop on CRO is shown below.

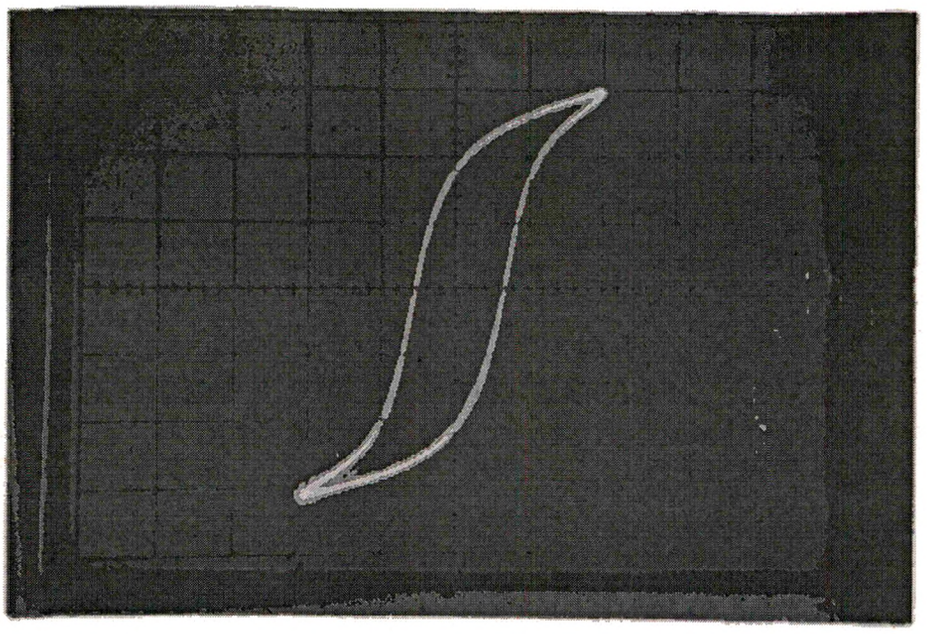

Photograph of hysterisis loop on CRO.

The vertical displacement along magnetization was noted. The calibration factor (C. F.) was calculated by following relation.

$$C.F. = \frac{\text{Total magnetization of Ni}}{\text{Vertical displacement on CRO}}$$

$$= \frac{53.34 \text{ x mass of Ni}}{\text{Vertical displacement volts}} \text{ emu/v} \qquad 3.5$$

The standard Ni was then replaced by individual sample successively and the displacements of each sample were noted. The standard magnetization was then calculated by following relation

σ_s = Vertical reading of sample x CF 3.6

$$\sigma_s = \frac{\sigma_s}{\text{Mass of the pellet}} \text{ emu/gm} \qquad 3.7$$

Saturation magnetization for given porosity was calculated from equation

$$M_S = (1 - P)\, dx\ \sigma_s' \qquad 3.8$$

Where

$$P = \frac{(dx - da)}{dx} \times 100$$ is the porosity

dx = X Ray density g/cc.

da = actual density g/cc.

The magnetic moment per molecular formula unit in Bhor magnetron (n_β) is given by

$$n_\beta = \frac{\text{Molecular weight of the sample}}{5585} \times \sigma_s' \qquad 3.9$$

5585 is due to product of the Avagadro's number and Bhor magnetron.

The magnetization data is tabulated in table 3.3.

Table 3.4 Magnetization data.

Composition	σ_s' (emu/gm)	$4\pi M_s$ (G)	M_r/M_s	n_β
$MgFe_2O_4$	19.62	607.5	0.6	0.7098
$Mg_{0.4}Mn_{0.5}Zn_{0.1}Al_{0.8}Fe_{1.2}O_4$	16.61	583.6	0.44	0.584

3.2.6 Initial permeability measurements

The initial permeability measurements were carried out on samples in torroid form using Hewllet Packard LCR meter as a function of temperature from room temperature to 600° C at a fixed frequency of 1 kHz. The initial permeability values were calculated using the following relation.

$$\mu_i = \frac{Ls\ (\mu H)}{0.0046\ N^2\ h\ \log\ (OD/ID)} \qquad 3.10$$

Ls = inductance in μH

N = Number of turns wound on torroid samples.

H = Thickness of the torroid in inches.

OD and ID are outer and inner diameters of the torroid samples.

Variation of initial permeability with respect to temperature and frequency is plotted in figure 3.5. From Figure 3.5 (a) it is seen that the permeability initially increases and at a particular temperature there is a sudden fall. Beyond this temperature the permeability is almost constant. The temperature at which there is sudden decrease in initial permeability is the Curie temperature. From the graph it is 600 K for $MgFe_2O_4$ and 465 K for $Mg_{0.4}Mn_{0.5}Zn_{0.1}Al_{0.8}Fe_{1.2}O_4$. These values match with those reported for similar ferrites using ceramic method. The sharp decrease in μ_i near Tc suggests the single-phase formation of the ferrite. This observation is supported by XRD patterns, which do not show impurity peaks. The

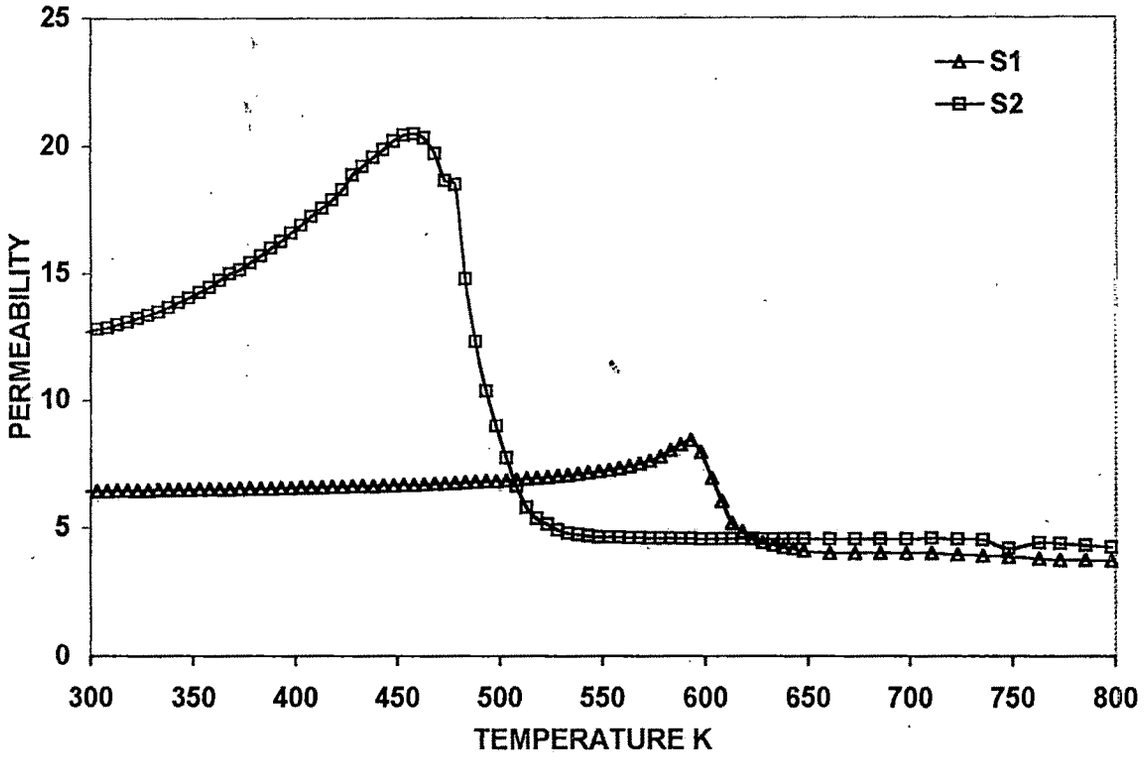

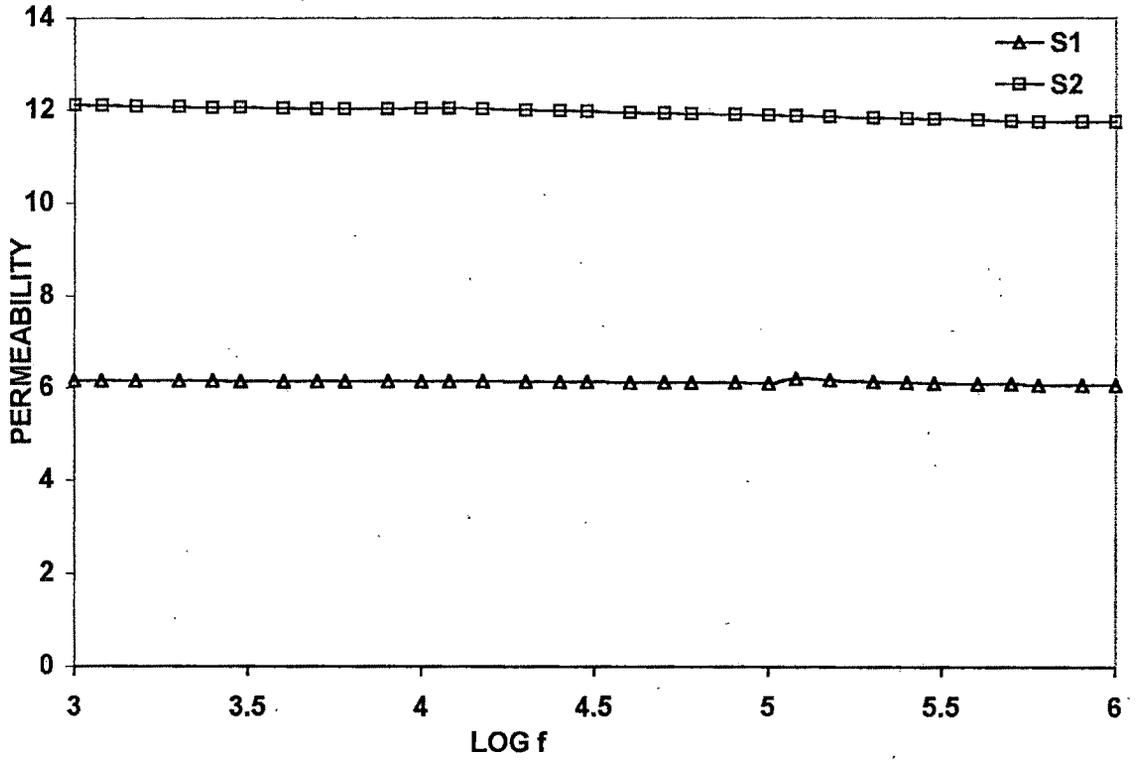

FIGURE 3.5(a,b) : Variation of initial permeability with respect to temperature and frequency.

verticality of the drop indicates increased chemical homogeneity and the slope of this drop provides an evaluation of this [86,87]. According to Arcos et al [86] lower μ_i indicate smaller grain size. The $MgFe_2O_4$ shows slightly smaller grain size than $Mg_{0.4}Mn_{0.5}Zn_{0.1}Al_{0.8}Fe_{1.2}O_4$.

From the graph of permeability verses log f it is seen that as frequency increases there is almost no change in permeability. The permeability of $Mg_{0.4}Mn_{0.5}Zn_{0.1}Al_{0.8}Fe_{1.2}O_4$ is higher than that of $MgFe_2O_4$. Others [88] have observed flat permeability profile upto 1 MHz for similar ferrites.

Sample S2 ($Mg_{0.4}Mn_{0.5}Zn_{0.1}Al_{0.8}Fe_{1.2}O_4$) has zinc in it. The effect of zinc content is similar to that of increasing the sintering temp whereby the initial permeability increases. Verma et al [89] have observed that increase in zink content increases the grain size, density and decreases the anisotropy which results in increase in the value of μ_i.

3.2.7 Dielectric properties.

The A. C. electrical measurements on ferrite sample in pellet form were carried out on Hewllet Packard LCR meter, in the frequency range of 1 KHz to 1 MHz at room temperature. The parameters viz. Capacitance (C), Loss tangent (tan δ) were recorded directly. The dielectric constant was calculated using the following relation.

$$\varepsilon' = \frac{C\,d}{\varepsilon_o\,A} \qquad 3.11$$

Where

d = Thickness of the pellet.

A = Area of free space.

$\varepsilon_o = 8.86 \times 10^{-5}$ is the permeability of free space.

Variation of dielectric constant with frequency is plotted in Figure 3.6. The dielectric constant decreases with increase in frequency for both the ferrites exhibiting normal ferrimagnetic behavior. The dielectric dispersion is observed in the low frequency region and it remains almost independent of

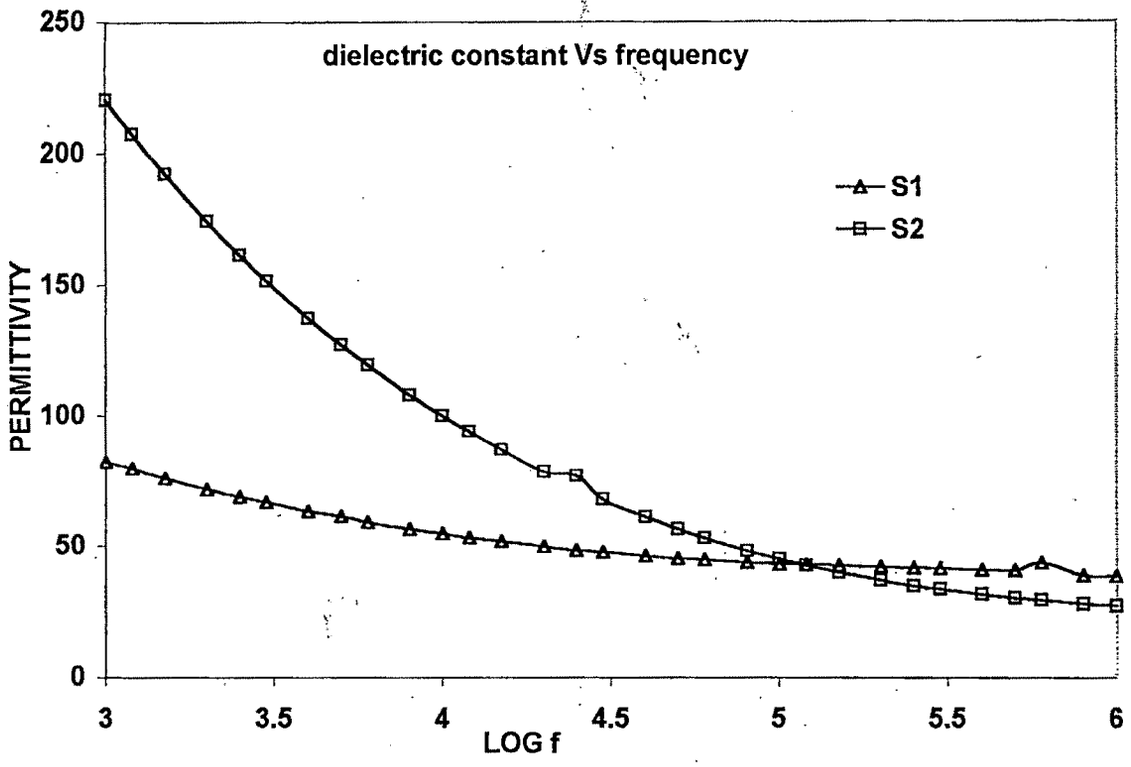

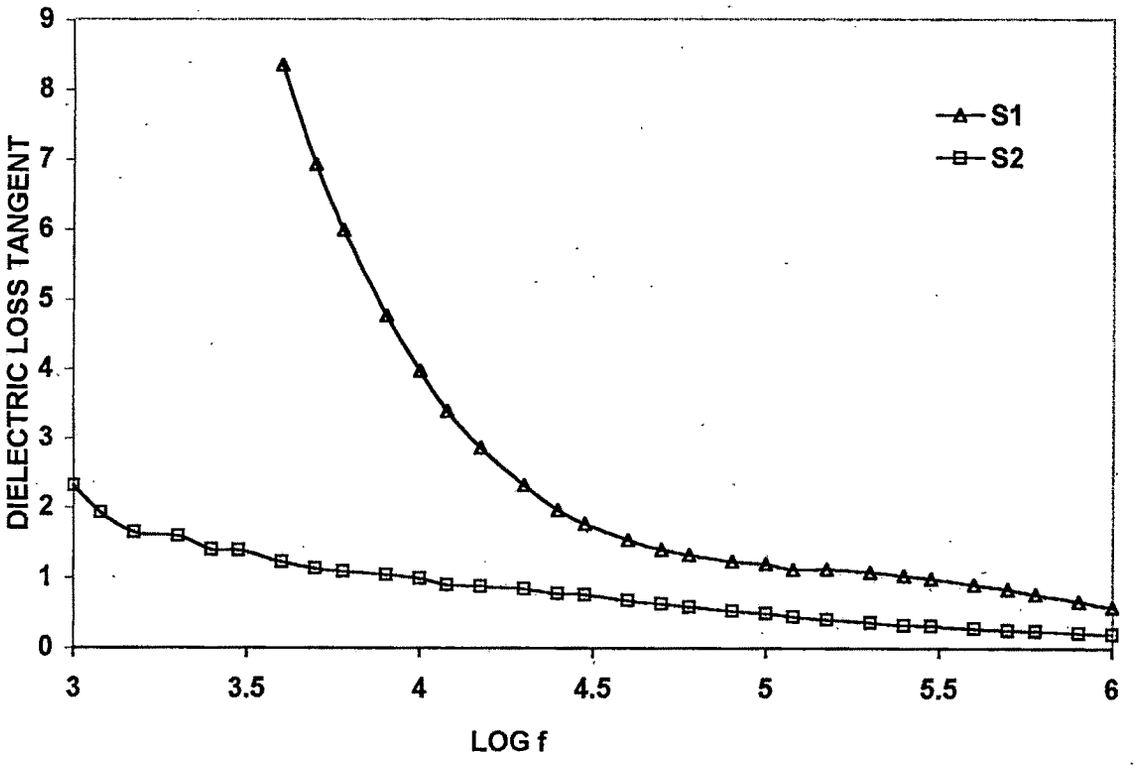

FIGURE 3.6 : Variation of dielectric constant and dielectric loss tangent as a function of Log f.

applied external field on the high frequency side. The dielectric dispersion is observed at the low frequency region is due to Maxwell – Wagner [90,91] type of interfacial polarization which is in good agreement with Koops phenomenological theory [92]. According to Koops, the ferrite can be regarded as a good dielectric material since it contains layers of highly conducting grains separated by bad conducting grain boundary. The large value of ε' at iower frequencies are due to the predominance of species like Fe^{+2} ions, interfacial dislocation pile ups, oxygen vacancies, grain boundary defects etc [90,91]. The decrease in ε' with frequency is because of the fact that any species contributing to polarizability are bound to show lagging behind the applied field at higher frequencies.

Variation of loss tangent with frequency is shown in Figure 3.6 (b). It is seen that tanδ decreases with frequency, it is very small at high frequency. The observed dispersion in tan δ can be explained with the help of following relation.

$$\tan \delta = \frac{1}{\omega \varepsilon_0 \varepsilon_r}$$

Where

ω = angular frequency corresponding to maximum value of tan δ.

3.3 Studies on EMC patch antenna.

The patch antenna was designed using designing equations given in chapter II. The metallization for patch and feed line was silver thick film. To the authors knowledge no reports are available on the investigation of silver thick film electromagnetically coupled patch antenna. The use of ferrite pellet overlay on this type of antenna has also been done for the first time. Two patches for different resonance frequencies 9.2 GHz and 10.4 GHz were designed. For each resonance frequencies four antenna patches long with two microstrip lines were fabricated. The results given in the following articles are the average of the four patches per resonance frequency. The variation from patch

to patch was less than 0.1 %. The EMC patch antenna with resonance frequency at 9.2 GHz is termed as patch 1 and the other one at 10.4 GHz as patch 2.

3.3.1 Measurement of resonance frequency of the antenna without Ferrite loading (overlay).

Initially the EMC patch antennas were investigated for their resonance frequencies for three feeding positions viz. Long Side Fed (LSF), Short Side Fed (SSF) and Diagonally Fed (DF). In these measurements output in mV was recorded for frequencies ranging from 8-12 GHz. Square law detector was used which detects power proportional to square of voltage.

Figure 3.7 (a) shows the graph of output as a function frequency of patch 1 for LSF, SSF and DF. Figure 3.7 (b) shows the same parameters for patch 2. Both the patches were designed considering feeding from long side. From Figure 3.7 (a) it is seen that patch 1 has resonance frequency at 9.2 GHz with 23 % power efficiency. For SSF and DF there is broad peak with low power efficiency. The resonance has shifted to lower frequency side. For SSF peak is from 8.1 GHz to 8.65 GHz with 7 % power efficiency. For DF power efficiency is very less. For all three feeding positions patch1 has no response for frequencies higher than 10 GHz.

From figure 3.7 (b) it is seen that for LSF of patch 2 resonance is at 10.4 GHz where power efficiency is 10 %. Two small peaks at 9.4 GHz are also observed. For SSF broadband peak from 8 GHz to 8.7 GHz has been observed which may be extending below 8 GHz. The power efficiency is 10 % that is comparable with LSF. In case of DF peak is at 8.2 GHz with very low power efficiency (3.5 %). Power efficiency is smallest (almost zero) at the frequencies higher than 9 GHz for SSF and DF.

3.3.2 Effect of ferrite pellet loading (overlay).

The effect of two aspects (i) thickness (ii) composition of the ferrite pellet as an overlay on the EMC patch antenna was studied. As already mentioned two

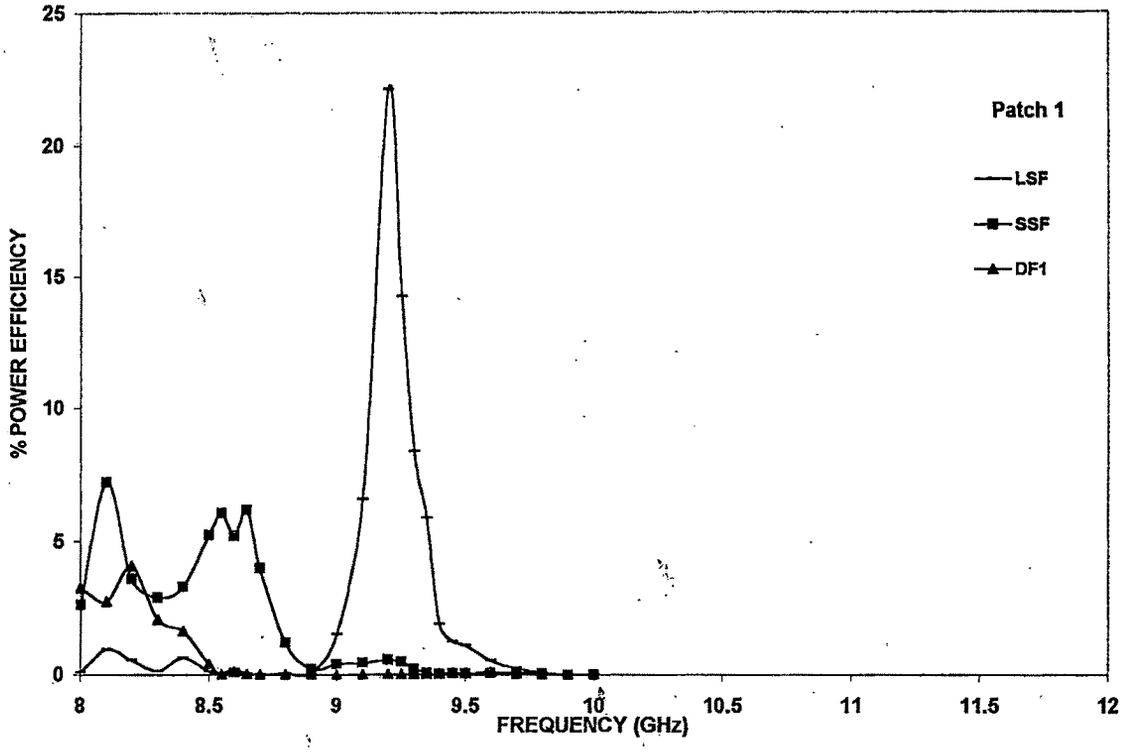

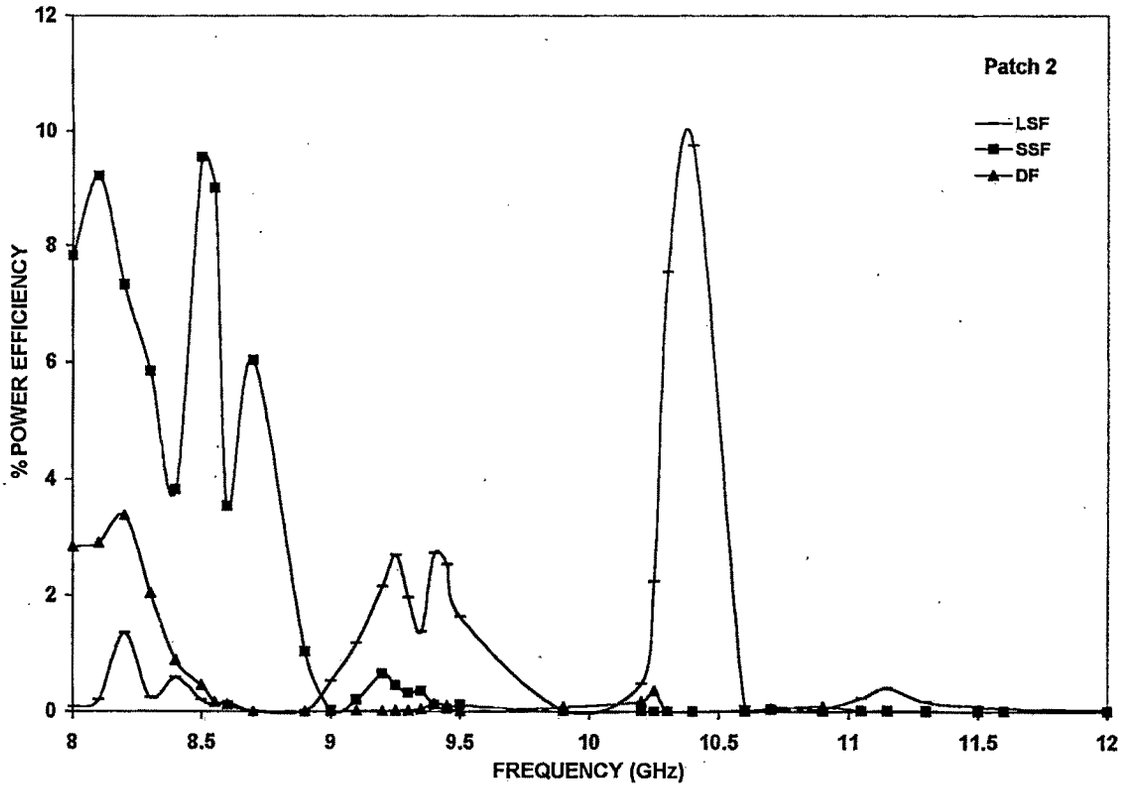

FIGURE 3.7(a,b) : Effect due to change in feeding positions of patch 1 and patch 2
LSF- Long Side Fed, SSF- Short Side Fed, DF- Diagonally Fed.

types of ferrites of composition, $MgFe_2O_4$ (S1) and $Mg_{0.4}Mn_{0.5}Zn_{0.1}Al_{0.8}Fe_{1.2}O_4$ (S2) were studied as overlay. Ferrite pellets of diameter 0.5 cm with thicknesses ranging from 1.5 mm to 14.5 mm were kept one by one on the center of patch such that it covers the whole patch. Output was recorded for frequencies ranging from 8 GHz to 12 GHz.

3.3.2.1 Effect on LSF antenna.

Fig 3.8, 3.9 (a, b) represents thickness dependent effects for LSF of patch 1 and patch 2 respectively. From the figures, it is seen that for both the compositions the effect of ferrite is to decrease the power efficiency at resonance frequency for both the patches. At lower off resonance frequency side, power efficiency increases due to overlay. Due to S2 patch 1 attains higher power efficiency than due to S1. Where as at resonance frequency both compositions give almost similar power efficiency when used as overlay on patch 2 at its resonance frequency.

From Figure 3.8 (a, b) it is seen that both S1 and S2 are used as overlay, the bandwidth at resonance increases (with respect to with out overlay band width). The tendency for double peak characteristics is more prominent due to S2 overlay. A small irregularity at 8.1 GHz increases into a peak due to overlay. At this frequency as thickness of the ferrite overlay increases the % power efficiency also increases for both the ferrite overlays.

From Figure 3.9 (a, b) it is seen that at resonance (10.4 GHz) and at off resonance the antenna shows composition dependent and thickness dependent effects. At 10.4 GHz due to S1 overlay the power efficiency was minimum and increased as the thickness of overlay increased, can be observed in Figure 3.9 (a). Due to S2 overlay, the minimum power efficiency was for 5.81 mm thick overlay and there was an oscillatory behavior due to increase in thickness. At 9.2 GHz, the irregularity in the antenna output gets enhanced and a power efficiency greater than the original without overlay power efficiency at resonance is obtained. At this frequency also composition and thickness dependent changes are observed. Smallest thickness of S1 has

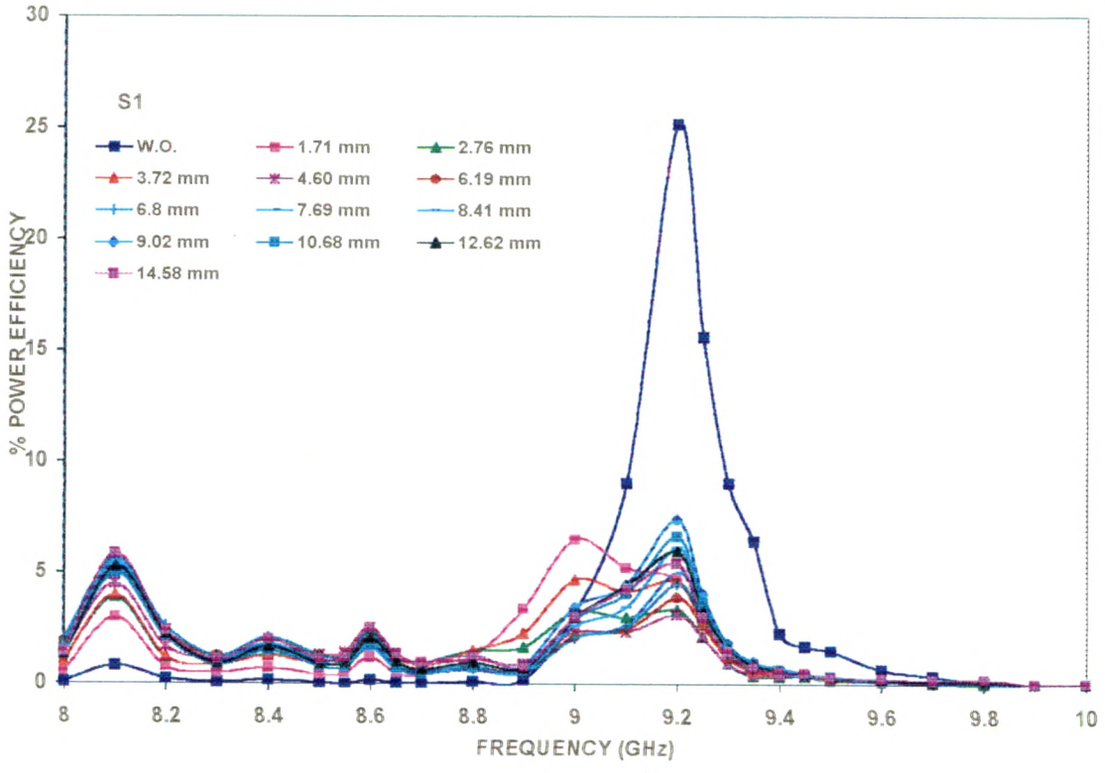

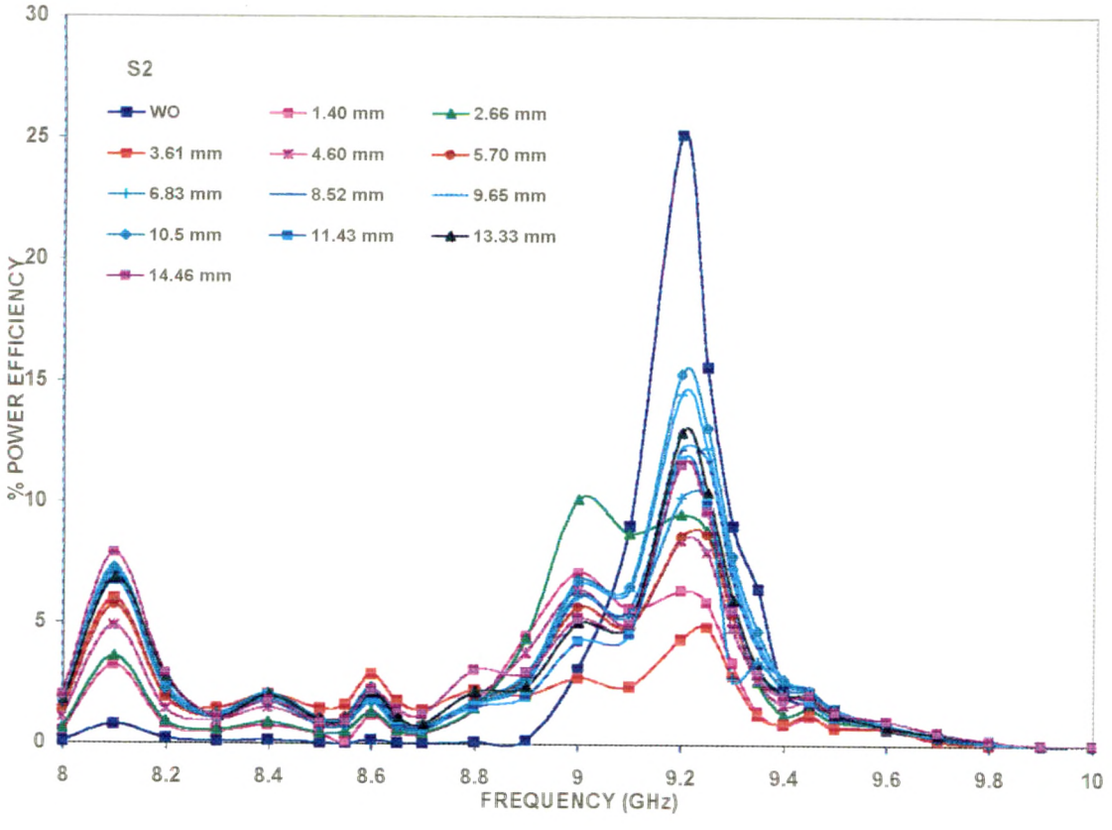

FIGURE 3.8(a,b) : Thickness and composition dependent ferrite loading effects on Long Side Fed patch1

S1- $MgFe_2O_4$, S2- $Mg_{0.4}Mn_{0.5}Zn_{0.1}Al_{0.8}Fe_{1.2}O_4$

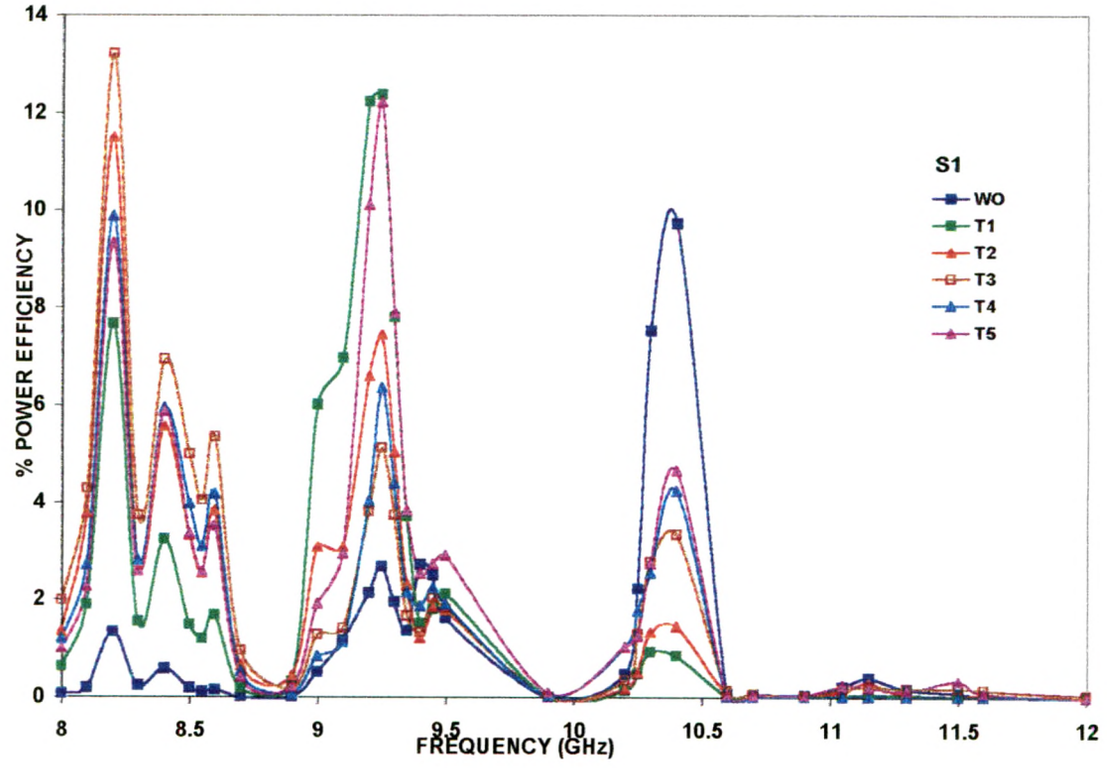

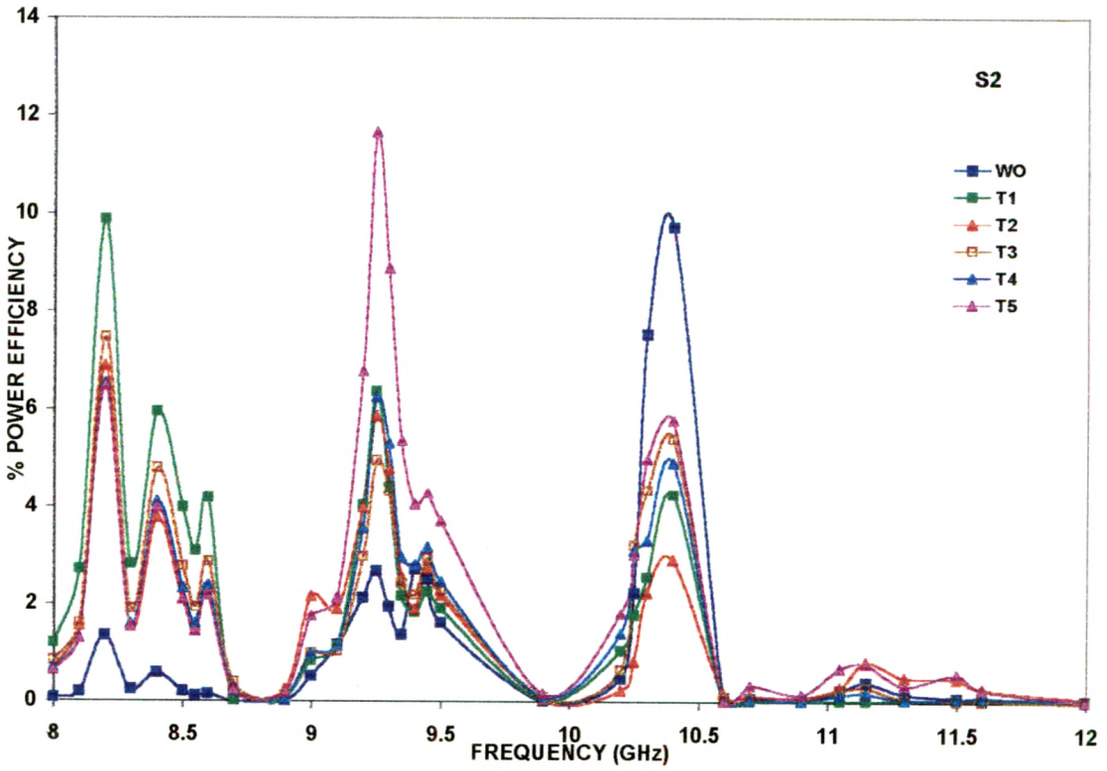

FIGURE 3.9(a,b) : Thickness(mm) and composition dependent ferrite loading effects on Long Side Fed patch 2

S1- $MgFe_2O_4$, S2- $Mg_{0.4}Mn_{0.5}Zn_{0.1}Al_{0.8}Fe_{1.2}O_4$

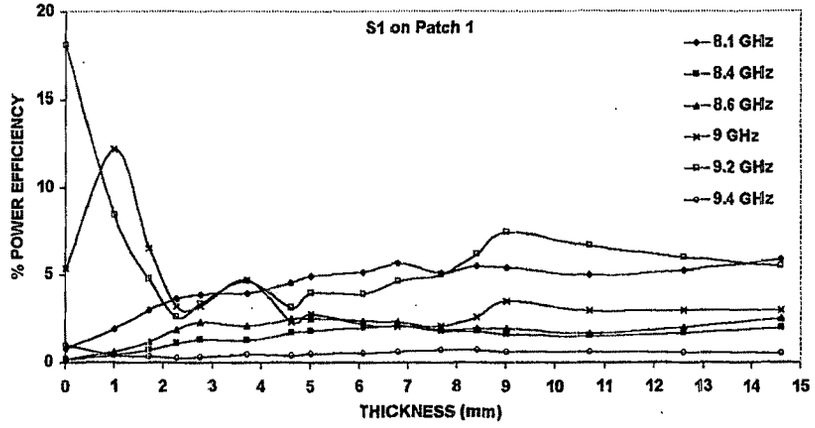

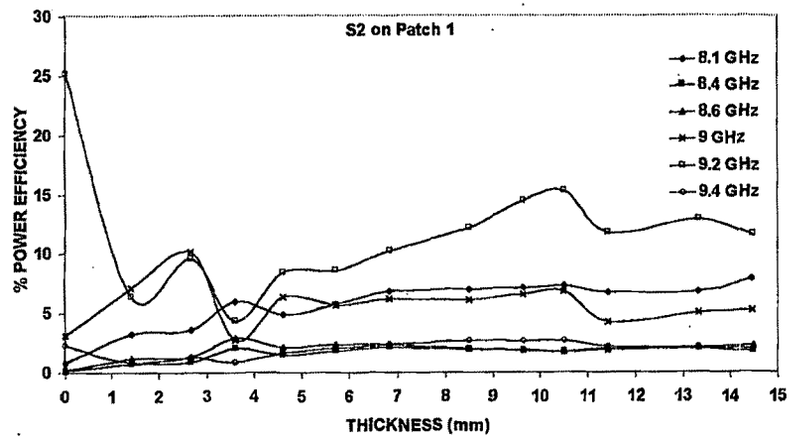

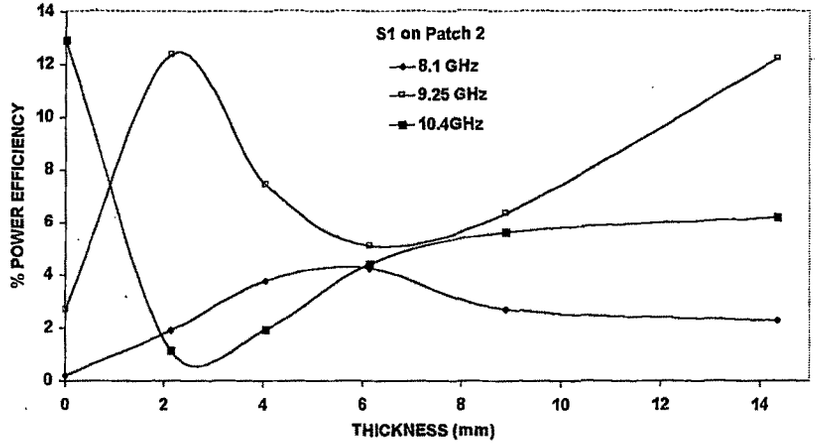

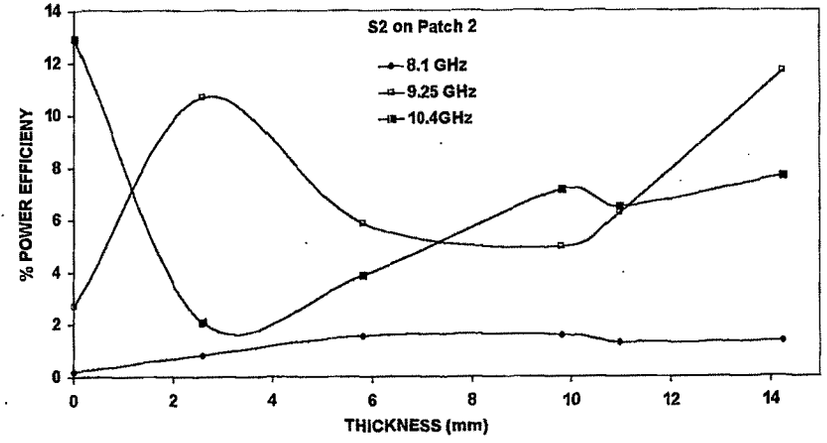

FIGURE 3.10 : Effect of change in thickness of ferrite loaded on Long Side Fed Patch 1 and Patch 2. S1- MgFe2O4, S2- $Mg_{0.4}Mn_{0.5}Zn_{0.1}Al_{0.8}Fe_{1.2}O_4$

maximum efficiency. It goes on decreasing up to 6 mm thick overlay and again increases for higher thicknesses such that 2 mm thick and 14 mm thick overlay has almost same power efficiency. At same frequency because of S2 from 2 mm to 9.8 mm thickness power efficiency goes on decreasing then increases for higher thicknesses. Overlay of 14 mm gives maximum power efficiency at 9.25 GHz.

At still lower frequency where there is a small irregularity at 8.2 GHz, due to both the ferrites as overlay there is a broad peak between 8.1 GHz and 8.6 GHz with three small maximums. When S1 is used as overlay the power efficiency goes on increasing up to 6.14 mm thickness after which the power efficiency is maximum for minimum thicknesses (that is for 2.58 mm) then it decreases for all the thicknesses greater than that.

In order to clearly depict the effect of thickness and composition of the ferrite overlay on patch 1 and patch 2, a graph of % power efficiency as a function of thickness has been plotted in figure 3.10.

3.3.2.2 Effect on SSF antenna.

Variation of % power efficiency as a function of frequency due to ferrite overlay when antenna is fed from short side (SSF) is shown in Figure 3.11 and 3.12 for patch 1 and patch 2 respectively. From Figure 3.11 (a, b) it is seen that there is shift in the resonance frequency due to both S 1 and S 2 overlay. Due to S1 as overlay (Figure 3.11 (a)), the humped nature of the curve of without overlay situation between 8.5 GHz to 8.7 GHz seems to have become two separate peaks at 8.2 GHz and 8.4 GHz. The peak at 8.1 GHz seems to have shifted to frequency lower than 8 GHz since the curve shows the tendency to have an increasing power efficiency profile. At 8.5 GHz (without overlay resonance position) as the thickness of S1 increases the power efficiency decreases till about 4.6 mm (1.9 %) after which it starts increasing linearly attaining a value of the order of 4.5 % for a thickness of 14.58 mm. Due to S2 overlay, more thickness dependent effects are observed. The peak at 8.5 GHz becomes increasingly prominent with thickness. Due to S2 overlay

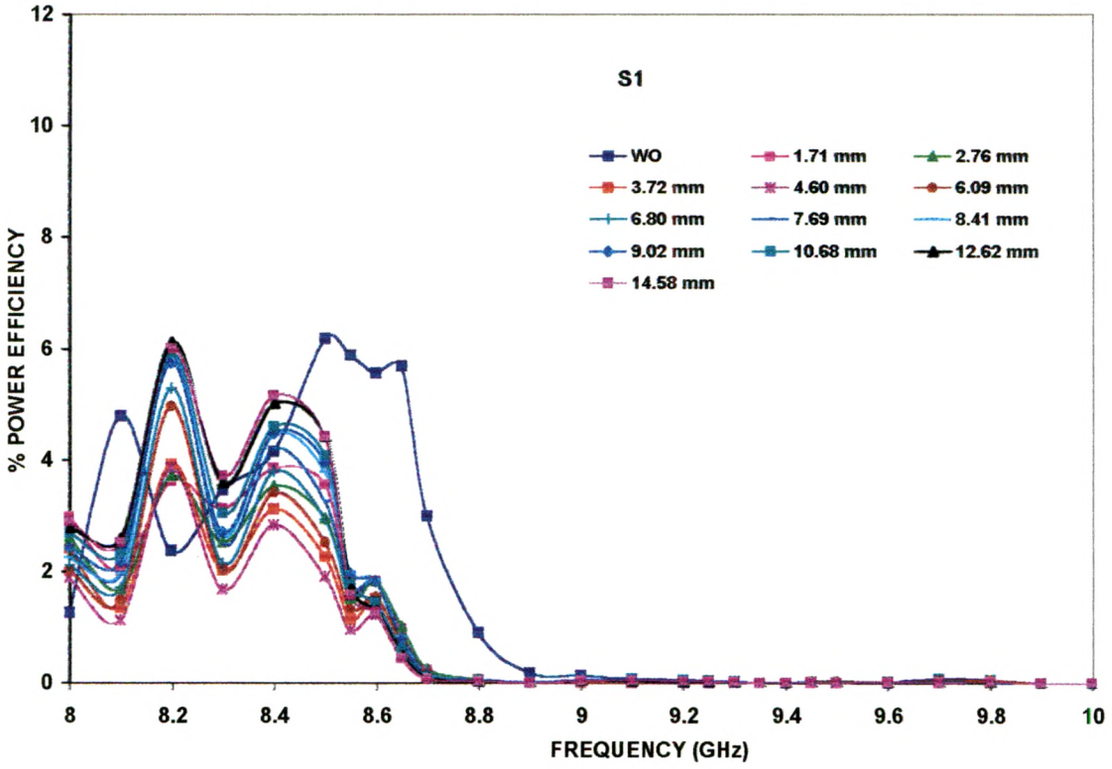

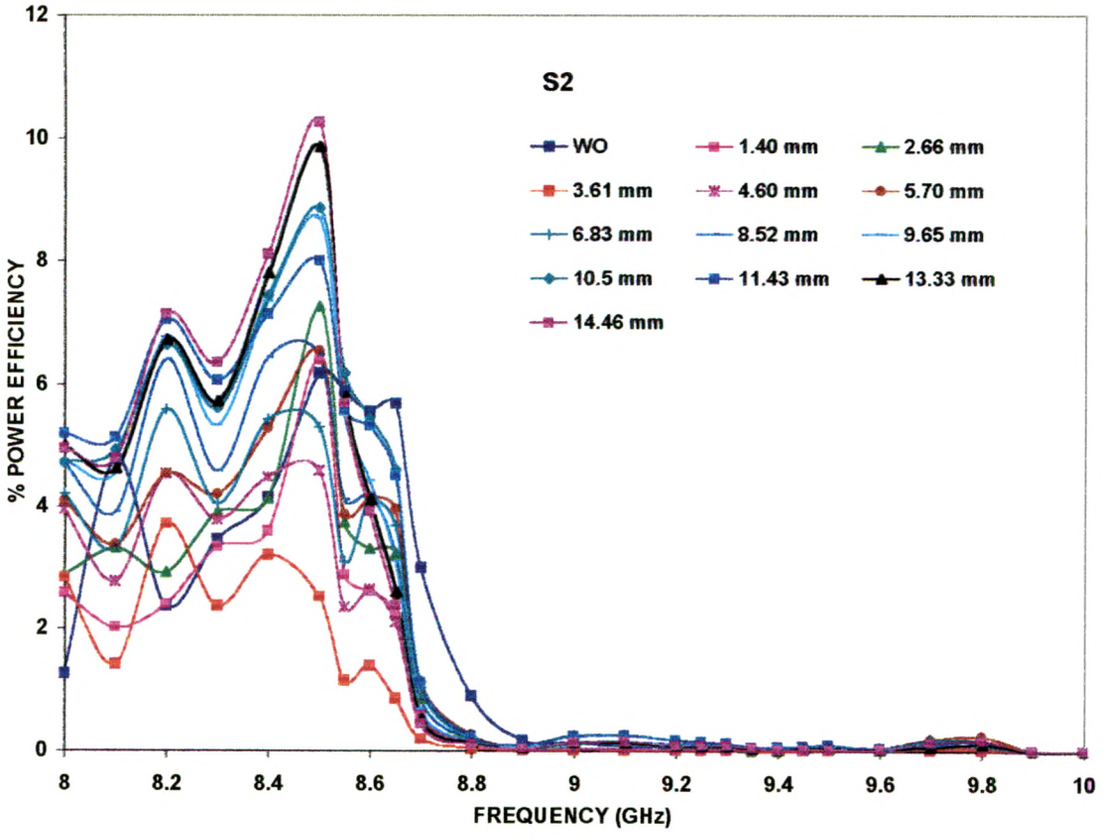

FIGURE 3.11(a,b) : Thickness and composition dependent ferrite loading effects on Short Side Fed patch

S1- $MgFe_2O_4$, S2- $Mg_{0.4}Mn_{0.5}Zn_{0.1}Al_{0.8}Fe_{1.2}O_4$

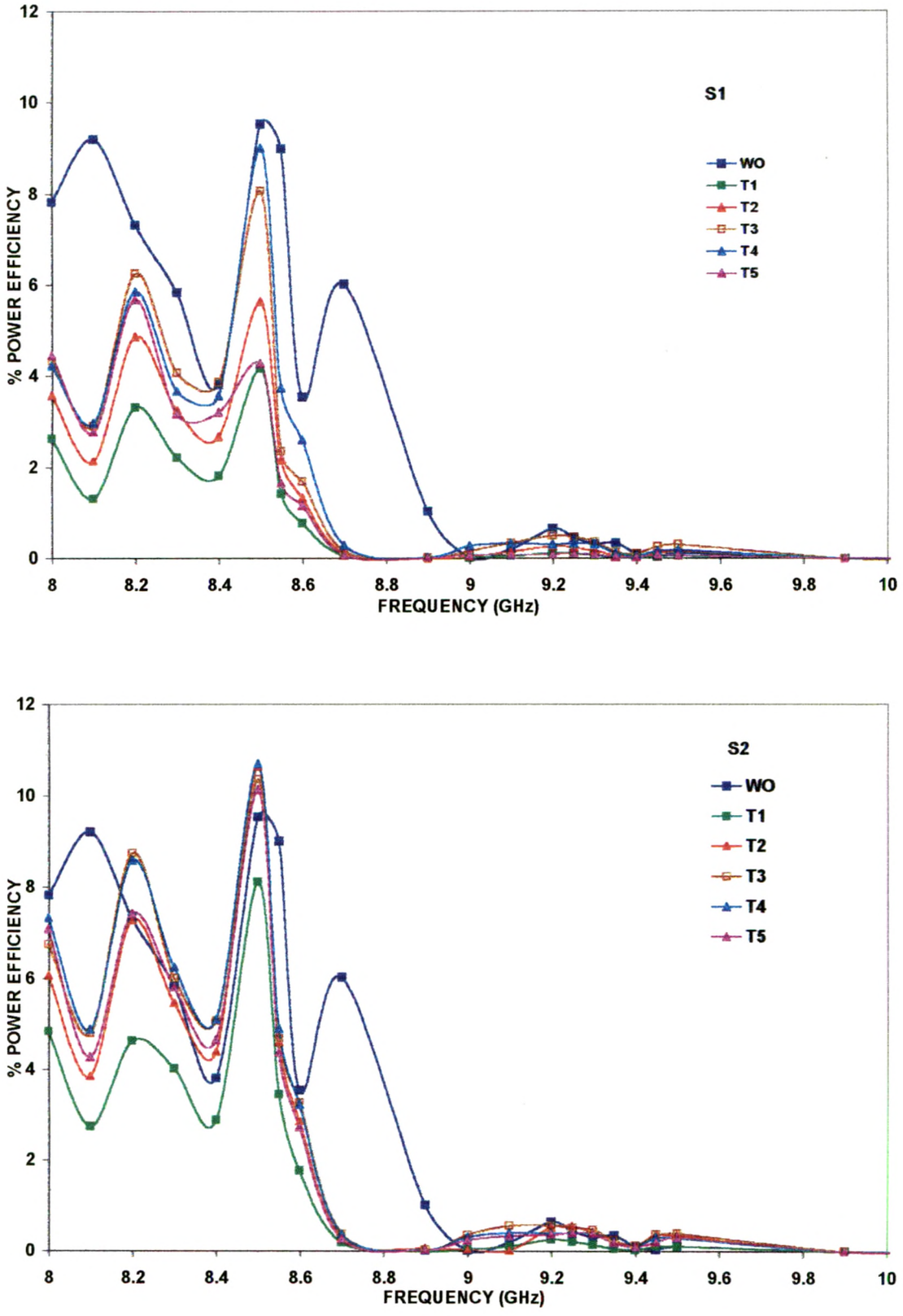

FIGURE 3.12(a,b) : Thickness(mm) and composition dependent ferrite loading effects on Short Side Fed patch 2

S1- $MgFe_2O_4$, S2- $Mg_{0.4}Mn_{0.5}Zn_{0.1}Al_{0.8}Fe_{1.2}O_4$

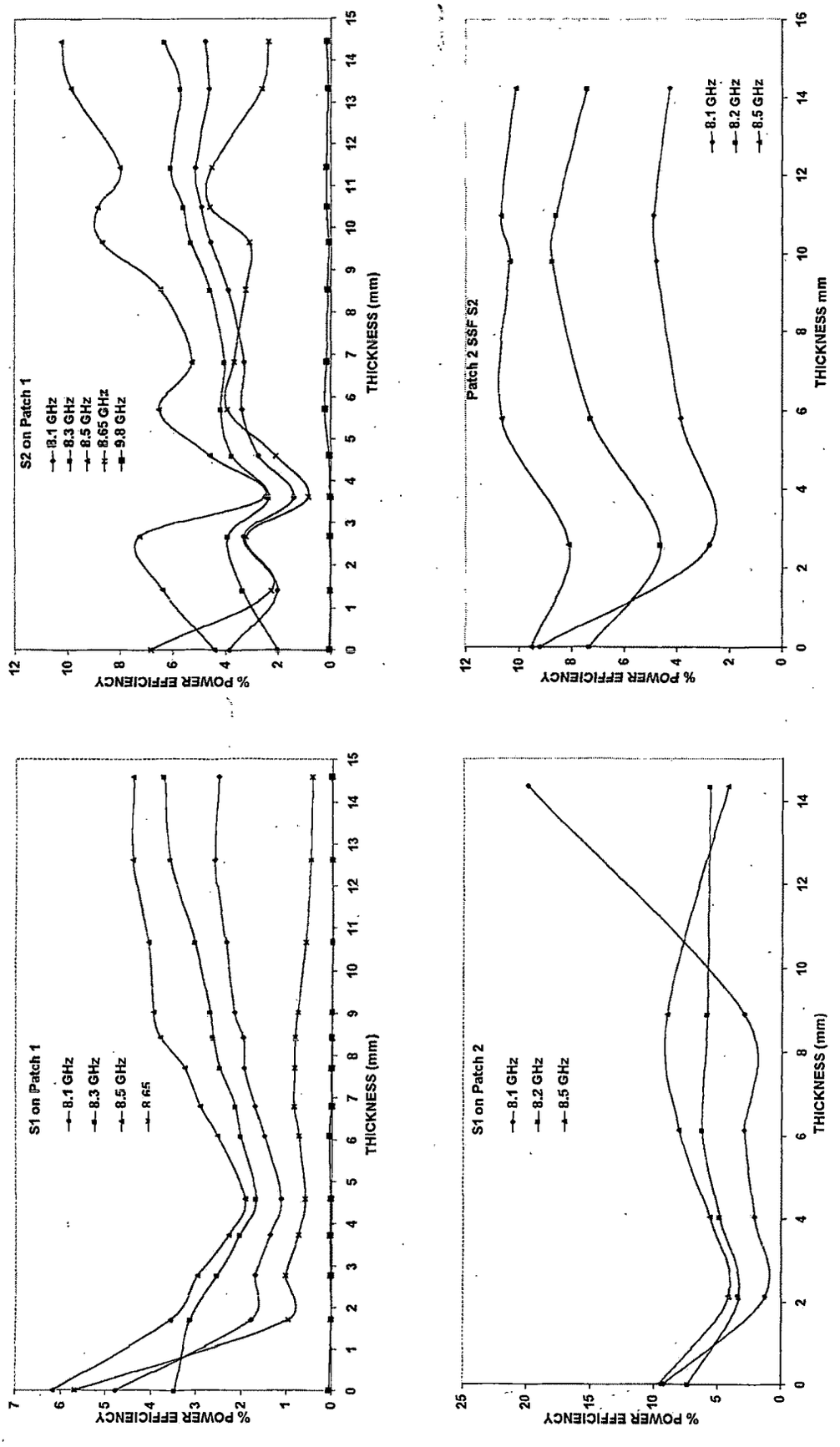

FIGURE 3.13 : Effect of change in thickness of ferrite overlay on Short Side Fed Patch 1 and Patch 2. S1- $MgFe_2O_4$, S2- $Mg_{0.4}Mn_{0.6}Zn_{0.1}Al_{0.8}Fe_{1.2}O_4$

the power efficiency varies nonlinearly at 8.5 and 8.2 GHz. At 9.8 GHz both the overlays gives zero power efficiency even the antenna without overlay has zero power efficiency.

From Figure 3.12 (a and b) it is seen that the peak at 8.7 GHz (without overlay) is suppressed due to overlay of both S1 and S2. There is indication that this has shifted to 8.5 GHz and the 8.5 GHz peak seems to have shifted to below 8 GHz. Thickness dependent variations are more prominent when S1 is used as overlay than for S2 overlay. The detailed effects of power efficiency as a function of thickness of overlay for SSF situation are depicted in Figure 3.13.

3.3.2.3 Effect on DF antenna.

The plots for the effect of various thickness of ferrite (S1 and S2) on the diagonally fed antennas are given in Figure 3.14 (a and b) and Figure 3.15 (a and b) for patch 1 and patch 2 respectively. Here also composition and thickness of ferrite overlay dependent effects are visible. Both the patch antennas have almost 0% power efficiency beyond 8.7 GHz without overlay. Due to both S1 and S2 overlay on both the patches, the power efficiency starts increasing in the 9-9.4 GHz range for patch 1 (Figure 3.14) and even up to 10.5 GHz for patch 2 for same thickness of overlay (Figure 3.15). Between broad peaks, the effect of overlay is to split the peak. This effect is more prominent in patch 1 than in patch 2. Nothing more can be said about patch 2, since the maxima seem to be extending below 8 GHz for which data is not available. Thickness dependent effects are more when S2 is used as overlay compared with S1 as a overlay.

Figure 3.16 gives the graph of % power efficiency as a function of thickness of the overlay, when the antenna is fed from diagonal side.

3.3.3 Radiation pattern measurements

From previous resonance frequency measurements, various frequencies were selected for radiation pattern measurements. The frequencies chosen were

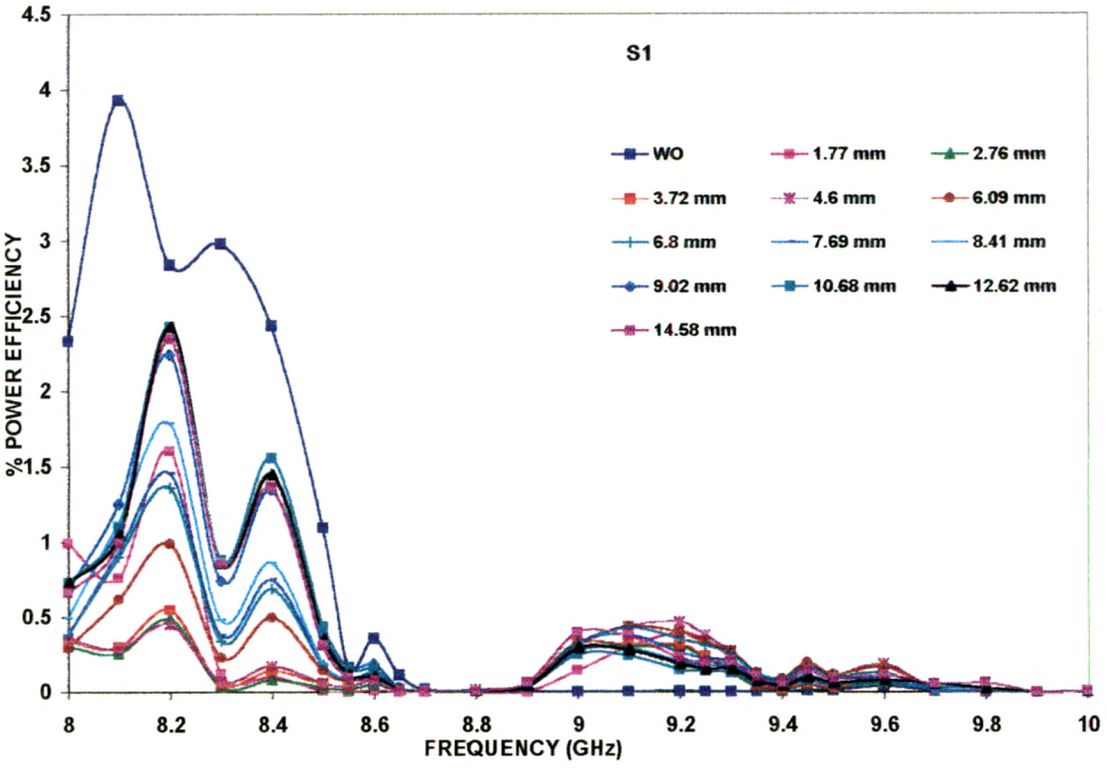

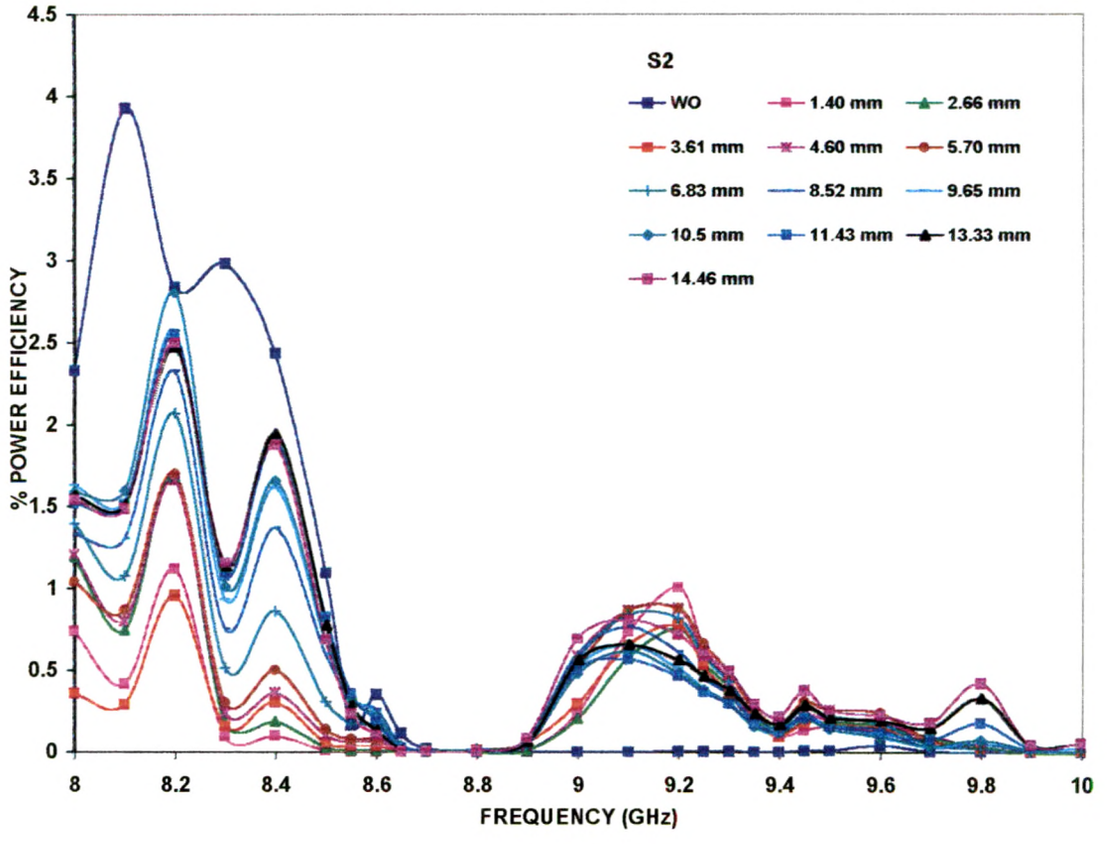

FIGURE 3.14(a,b) : Thickness and composition dependent ferrite loading effects on Diagonally Fed patch1

S1- $MgFe_2O_4$, S2- $Mg_{0.4}Mn_{0.5}Zn_{0.1}Al_{0.8}Fe_{1.2}O_4$

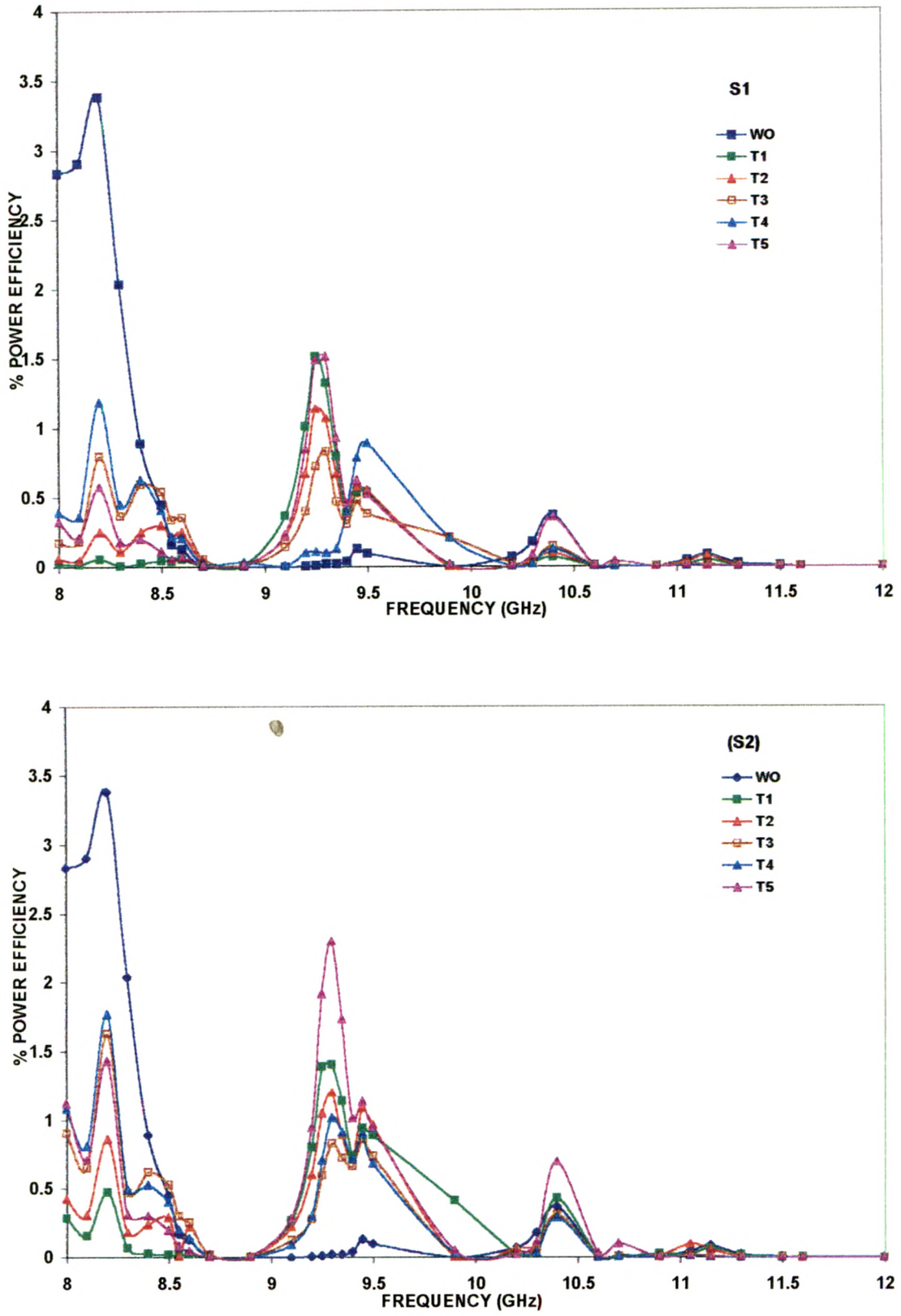

FIGURE 3.15(a,b) : Thickness(mm) and composition dependent ferrite loading effects on Diagonally Fed patch 2

S1- $MgFe_2O_4$, S2- $Mg_{0.4}Mn_{0.5}Zn_{0.1}Al_{0.8}Fe_{1.2}O_4$

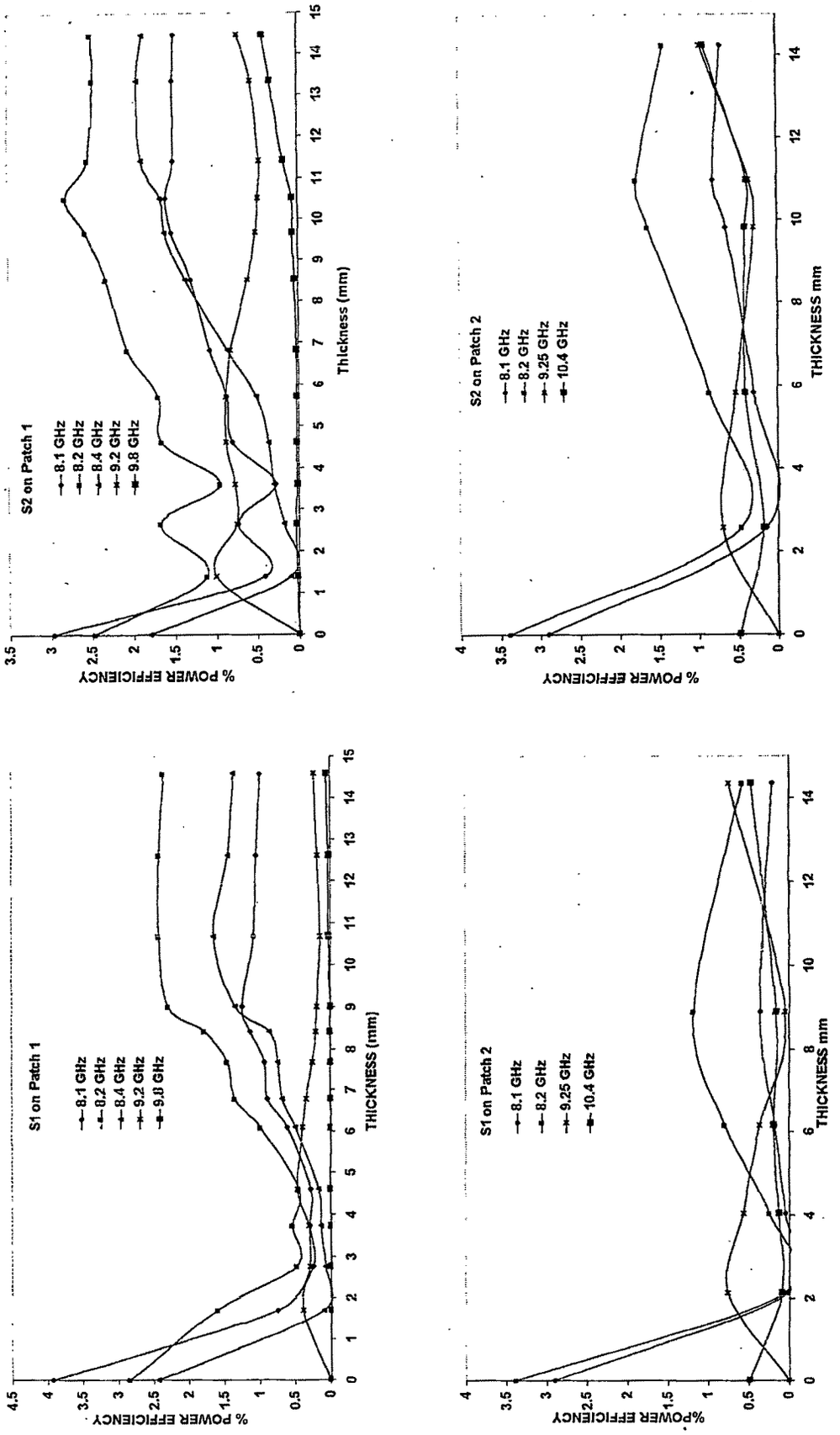

FIGURE 3.16 : Effect of change in thickness of ferrite overlay on Diagonally Fed Patch 1 and Patch 2. S1- $MgFe_2O_4$, S2- $Mg_{0.4}Mn_{0.6}Zn_{0.1}Al_{0.8}Fe_{1.2}O_4$

resonance frequency, lower off resonance frequency and higher off resonance frequency for three feeding positions. For radiation-pattern, measurement the horn antenna was rotated as described below. Horn antenna was rotated around patch antenna through 180^{O} keeping distance between them constant. For H plane horn was rotated in ZY plane and for E plane it was rotated in ZX plane. The power was recorded for every angle with difference of 10^{0}. From this Relative Power (R.P.) in dB was calculated. Radiation pattern is a variation of R.P. as a function of angle. Half power beam width can be obtained from radiation pattern. Directivity and gain can also be calculated.

3.3.3.1 Radiation patterns for LSF.

The radiation patterns in E and H planes with and without overlay on patch 1 and patch 2 for long side feeding position are shown in figure 3.17 and Figure 3.18 respectively. For the patch 1 two frequencies 9.2 GHz and 8.1 GHz were selected similarly for patch 2, along with these two frequencies 10.4 GHz was also studied.

From the Figures it is seen that the H plane patterns are broad and symmetric compared to E plane patterns. For all the frequencies studied the maximum radiated power is at $\theta = 0$. From Figure 3.17 it is seen that the E plane pattern at 9.2 GHz (resonance frequency of patch antenna) is highly non symmetric both with and without overlay of ferrite. There is not much thickness dependent and composition effects observed.

At $\theta = 50^{0}$the relative power (R.P.) goes to – 48dB due to overlay of S1 whereas with S2 overlay no detectable change is observed. At the same frequency the H plane pattern remains symmetrical due to thin overlay without much change in R.P. values. For higher thicknesses (S1 = 14 mm) there is rapid decrease in RP after 40^{0}. At 8.1 GHz, the E plane pattern is less nonsymmetrical than at 9.2 GHz. Two side lobes are visible at around 50^{0} and -60^{0}. The maximum R.P. has shifted to -10^{0} instead of 0^{0} at 9.2 GHz. Due to overlay of both S1 and S2 the RP has increased and the E plane pattern shows

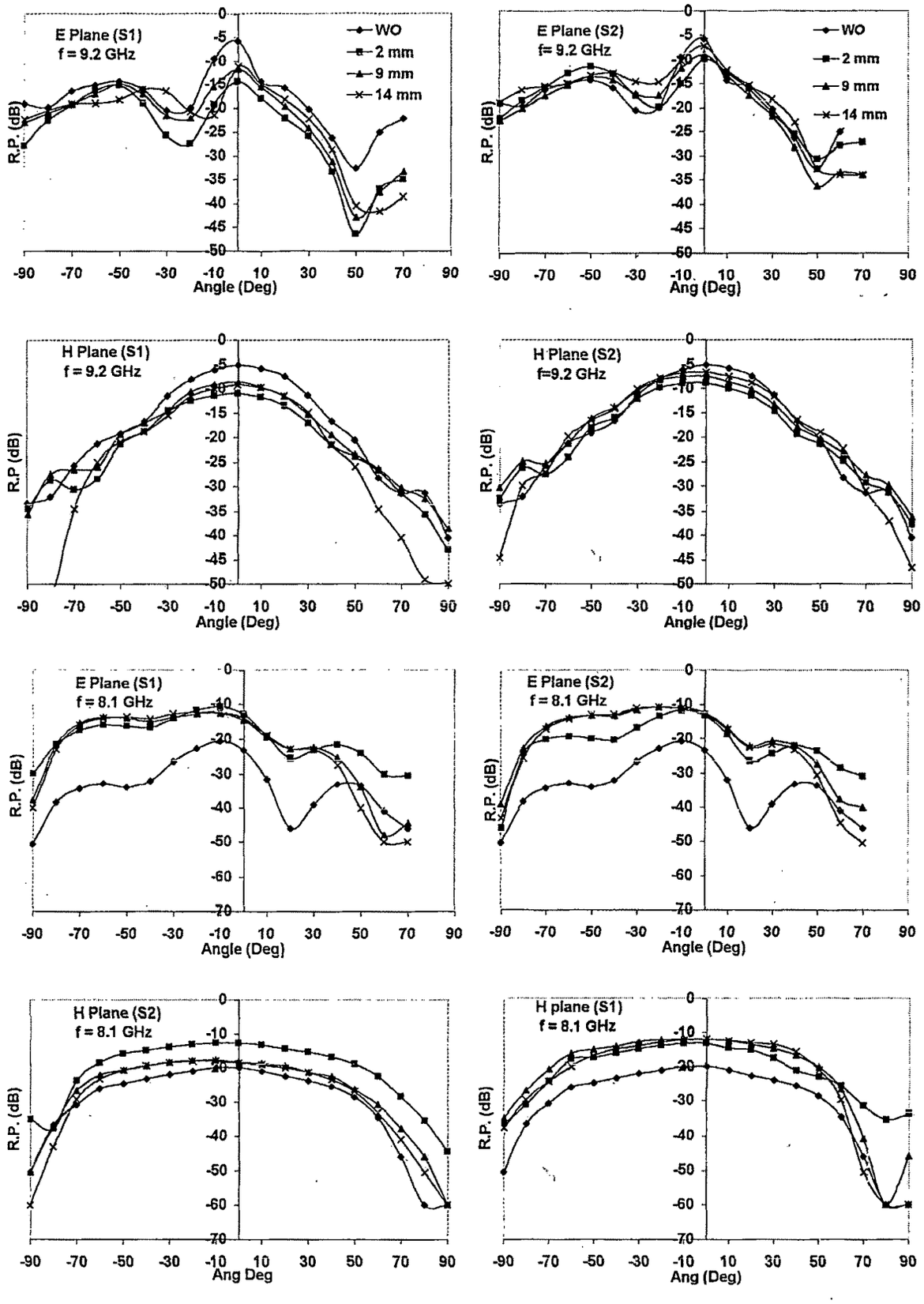

FIGURE 3.17 : E-Plane H-Plane Radiation patterns of Long Side Fed Patch 1. S1- $MgFe_2O_4$, S2- $Mg_{0.4}Mn_{0.5}Zn_{0.1}Al_{0.8}Fe_{1.2}O_4$

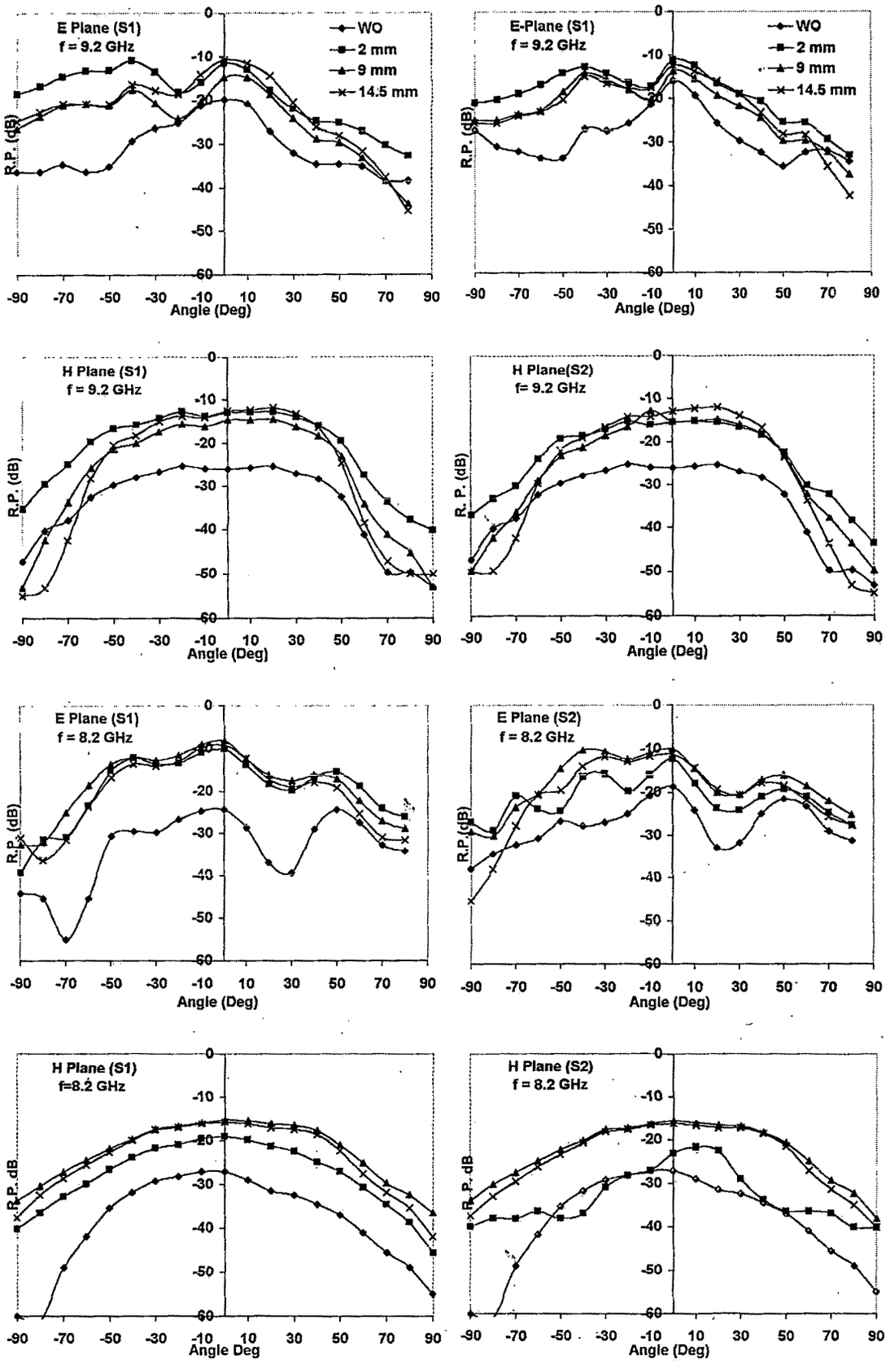

FIGURE 3.18: E- Plane, H-Plane Radiation patterms of Long Side Fed Patch - 2.
S1- $MgFe_2O_4$, S2- $Mg_{0.4}Mn_{0.5}Zn_{0.1}Al_{0.8}Fe_{1.2}O_4$

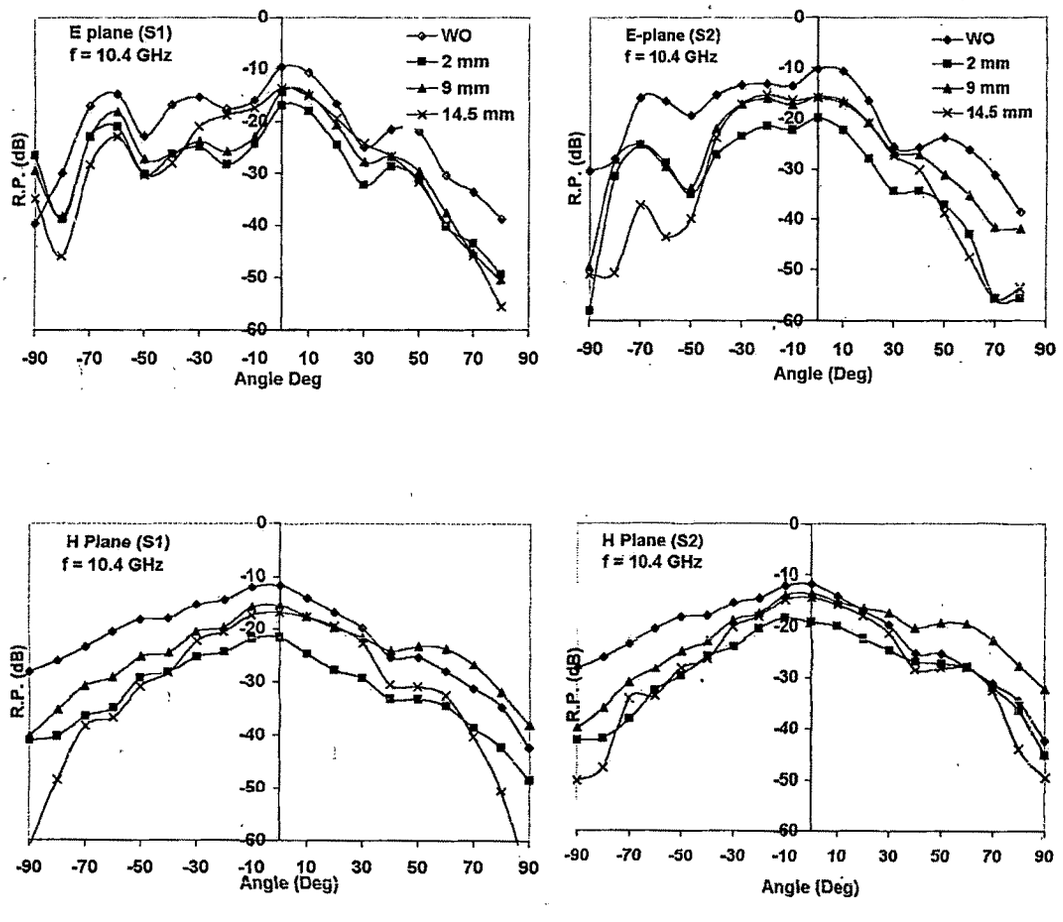

FIGURE 3.18: E- Plane, H-Plane Radiation patterms of Long Side Fed Patch - 2.
S1- $MgFe_2O_4$, S2- $Mg_{0.4}Mn_{0.5}Zn_{0.1}Al_{0.8}Fe_{1.2}O_4$

a tendency to be symmetrical and broad. The side lobes are lesser distinct than before. As thickness of overlay increases this smoothening of side lobes is more prominent.

The H plane pattern at 8.1 GHz is broader than that at 9.1 GHz. Due to overlay the R.P. increases and thickness dependent effects seen more due to S1 overlay.

From Figure 3.18 (patch 2) it is seen that the E plane pattern is more symmetrical at 9.2 GHz as compared to 8.2 GHz. The overlay increases the radiated power considerably for almost all the angles. The H plane patterns at both the frequencies are symmetrical. The overlay increases the R.P. The beam width decreases at 9.2 GHz and increases at 8.2 GHz. At 8.2 GHz due to S2 of thickness, 2 mm the H plane radiation pattern becomes narrow and the maximum R.P. shifts to approximately 10^0. At the resonance frequency of patch 2 that is at 10.4 GHz, side lobes are visible in E plane pattern, which are also present due to S1 and S2 overlay. The H plane pattern at this frequency has become slightly non symmetric. Due to S1 as overlay the pattern becomes more symmetrical; whereas with S2 as overlay the nonsymmetrical nature is retained.

3.3.3.2 Radiation pattern for SSF.

Figure 3.19 and 3.20 depicts the radiation patterns of patch 1 and patch 2 respectively, when fed from short side. Here also the H plane patterns are more symmetrical and broader than E plane pattern for both the patches without overlay. Due to overlay of S1 and S2 the radiated power decreases more at 8.65 GHz than at 8.1 GHz (Figure 3.19). Between 30^0 and 50^0 the relative power decreases sharply, after 50^0, the relative power increases when S1 of thickness 9 mm and 14 mm are used as overlay. One the other hand for 2 mm thick overlay it remains constant. When S2 is used as a overlay the sharp decrease is observed for 2 mm thick overlay but for other thickness the decrease is not that drastic. The H plane pattern does not show any thickness

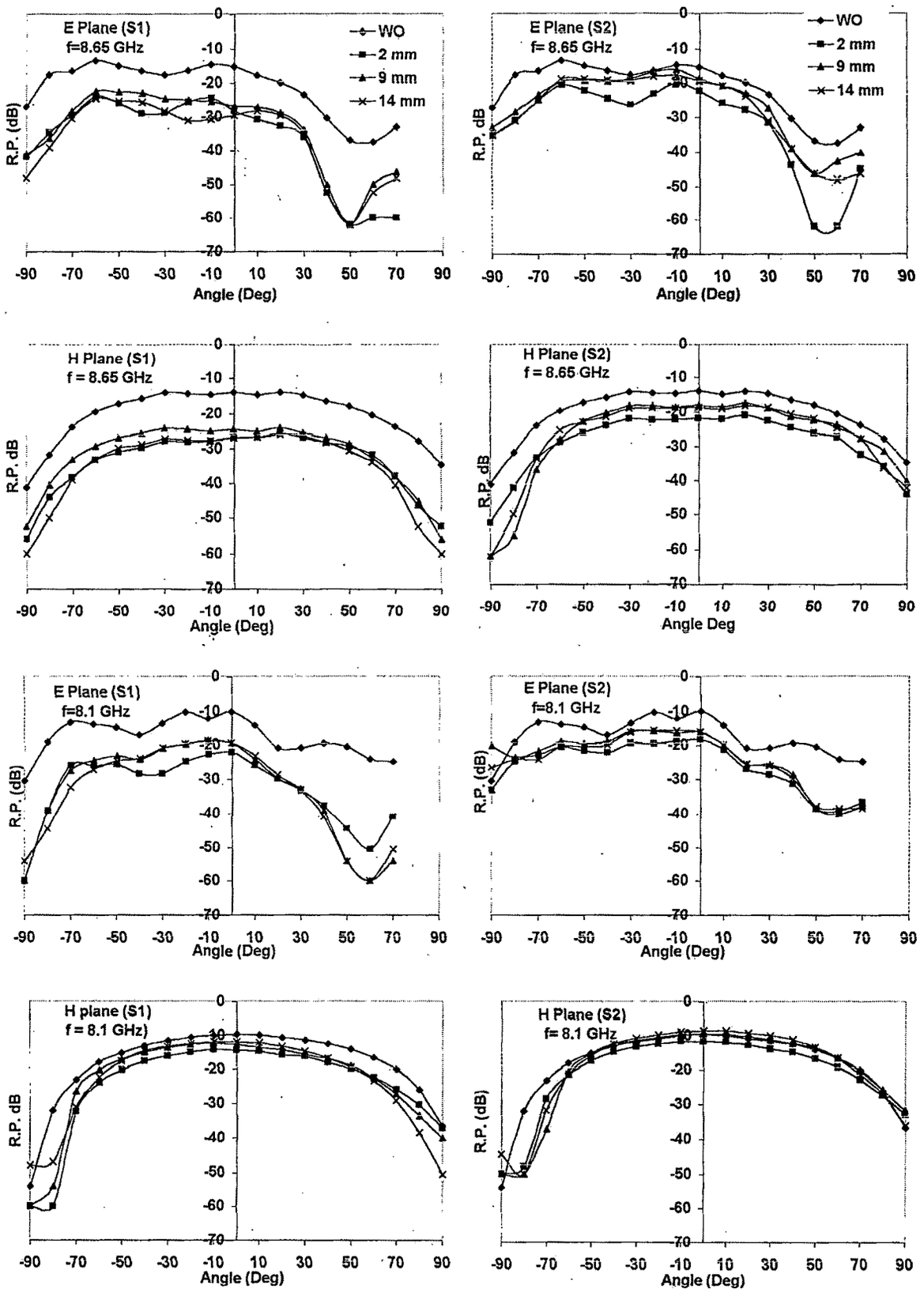

FIGURE 3.19 : E-Plane, H-Plane Radiation patterns of Short Side Fed Patch 1. S1- $MgFe_2O_4$, S2- $Mg_{0.4}Mn_{0.5}Zn_{0.1}Al_{0.8}Fe_{1.2}O_4$

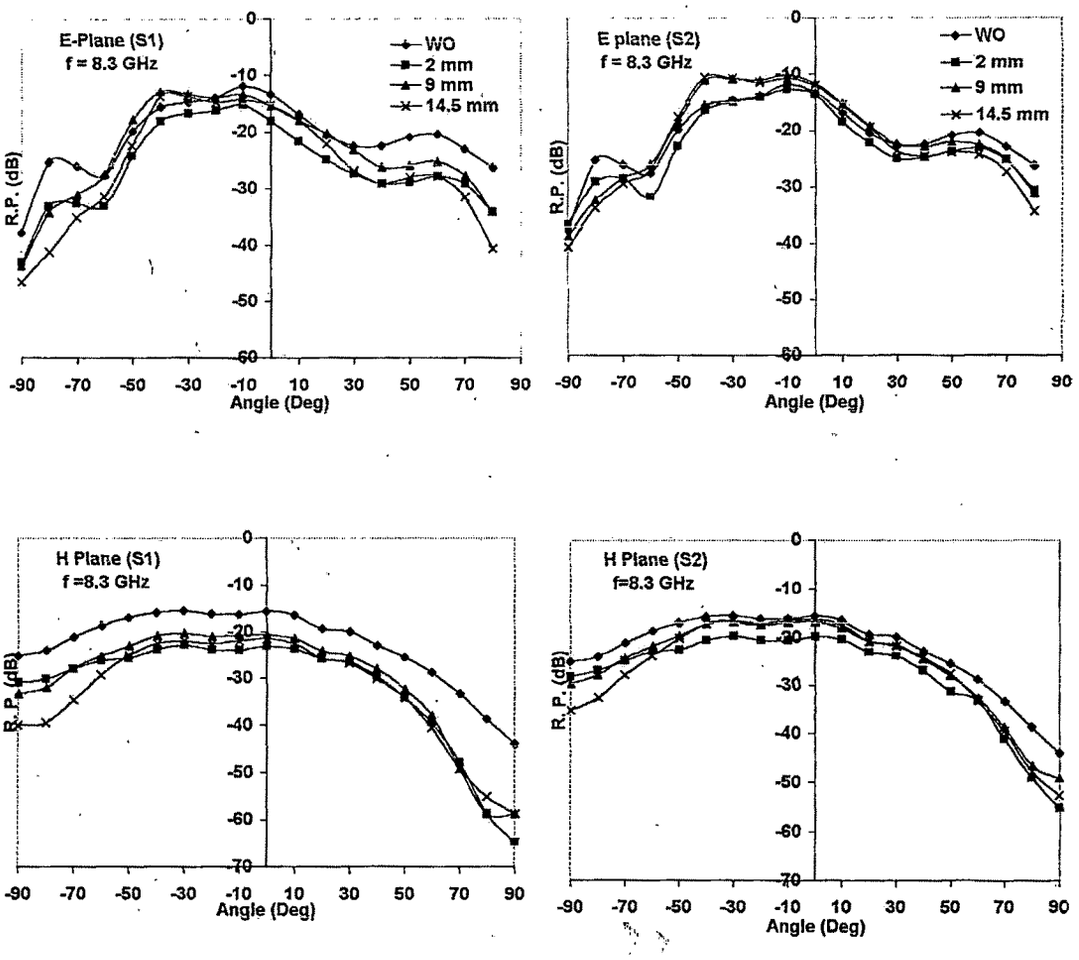

FIGURE 3.20: E- Plane, H-Plane Radiation patterns of Short Side Fed Patch - 2.
S1- $MgFe_2O_4$, S2- $Mg_{0.4}Mn_{0.5}Zn_{0.1}Al_{0.8}Fe_{1.2}O_4$

or composition dependent changes. At 8.1 GHz, similar effects are observed though S1 of smaller thickness also gives higher relative power after 60^0.

For patch 2 (Figure 3.20) the radiation patterns due to overlays follows the R.P. due to without overlay nature. The tendency for side formation at 60^0 and -80^0 is more prominent here. The H plane radiation pattern decreases more rapidly with increase in θ in the positive θ direction than in the negative θ direction. Due to S1 and S2 the changes in R.P. are the same.

3.3.3.3 Radiation pattern of DF.

Figure 3.21 and Figure 3.22 gives the radiation pattern of the patch 1 and patch 2 respectively when fed diagonally. From Figure 3.21 it is seen that the relative power at 9.2 GHz is below –50 dB and is highly nonsymmetrical in E plane. Due to overlay of S1 and S2 the R.P. increases to between –25 dB to –35 dB from -30^0 to $+30^0$ angular width in the H plane. In the E plane the R.P. is below –30 dB. The main lobe shifts to 10^0 due to S1 of thickness 2 mm and due to other thickness maximum is at 0^0. Side lobe appears at -50^0 with the R.P. of – 30 dB for S1 of 2 mm thick. Due to S2 a broad lobe appears between -50^0 and -70^0 with a R.P. of –30 dB. Below –40dB R.P. is as good as antenna is not radiating any power. At 8.1 GHz, though the E plane pattern is nonsymmetrical, the R.P. has risen to –18 dB without overlay at 0^0. Existence of sharp side lobe is evident at -70^0. On the positive θ side the R.P. is almost constant from 20^0 to 80^0. Due to overlay of S1 of thickness 2 mm the R.P. becomes very less (less than –40 dB). For the other two thicknesses the main lobe maxima is at -10^0 with R.P. of the order of – 25 dB. On the positive θ side the R.P. decreases with angle. On the negative θ side, side lobe becomes broader due to overlay; whereas due to S2 though there is decrease in R.P. the decrease is only of the order of –15 dB for S2 of thickness 2 mm. The maxima have shifted to 30^0 from no overlay situation. For higher thickness of S2 overlay the maxima is at -10^0. On both sides of maxima the

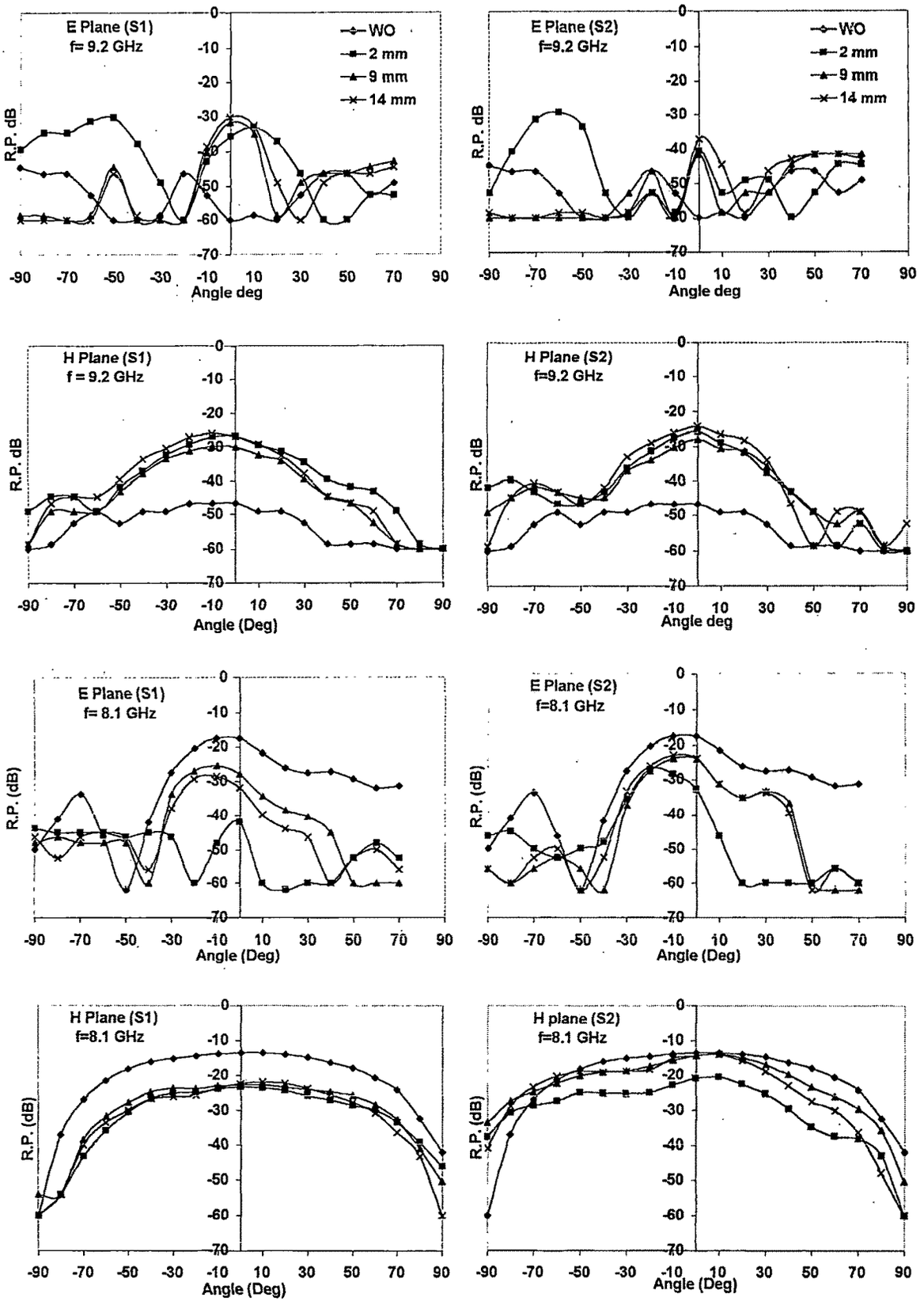

FIGURE 3.21 : E-Plane, H-Plane Radiation patterns of Diagonally Fed Patch 1. S1- $MgFe_2O_4$, S2- $Mg_{0.4}Mn_{0.5}Zn_{0.1}Al_{0.8}Fe_{1.2}O_4$

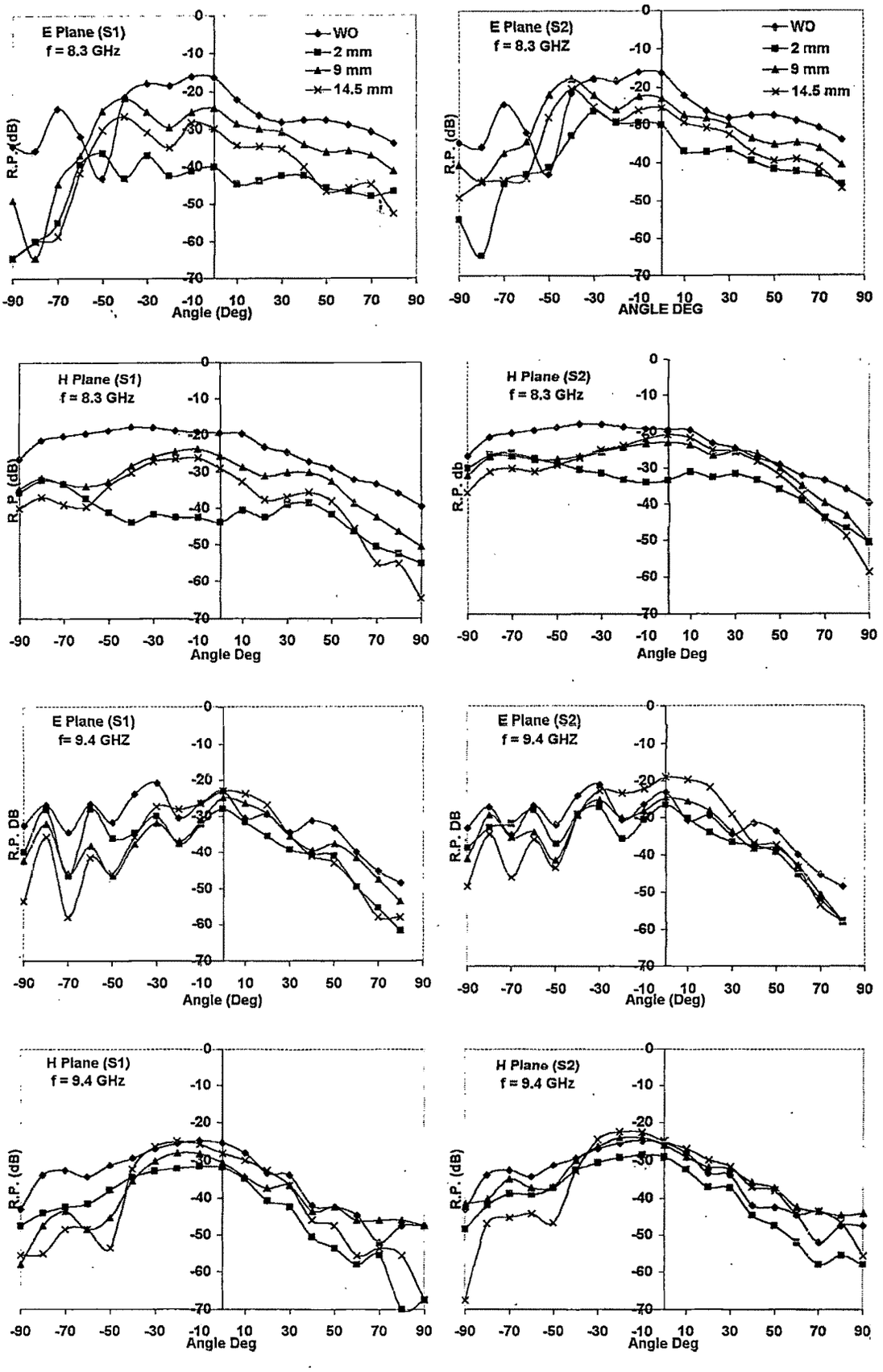

FIGURE 3.22: E- Plane, H-Plane Radiation patterns of Diagonally Fed Patch - 2.
S1- $MgFe_2O_4$, S2- $Mg_{0.4}Mn_{0.5}Zn_{0.1}Al_{0.8}Fe_{1.2}O_4$

R.P. decreases with increase in θ. Except for decrease in R.P the H plane radiation pattern does not change much due to either S1 or S2 overlay.

From Figure 3.22 (patch 2) it is observed that the E plane pattern shows a sharp side lobe at -80^0 at 8.3 GHz. Due to S1 overlay of thickness 2 mm the radiated power decreases from –.18 dB at 0^0 to –40 dB. Through all the range of angular variation, the R.P. is near that range. Beyond -60^0 a further sharp decrease is observed. For other thickness of overlay also the main lobe R.P. decreases and has a tendency to split giving other maxima at -40^0. On positive θ side there is tendency of double humped main lobe due to overlay. The side lobe at -80^0 disappears due to overlay of both types. At 8.3 GHz the H plane pattern shows constant Relative power (R.P.) from 0^0 to -80^0 and continuously decreasing R.P. from 0^0 to $+ 80^0$. The overlaid antenna with high overlay thickness of both types tend to decrease the beam width, whereas due to the lower thickness overlay the antenna follows the same pattern as without overlay pattern with decreased R.P.

At 9.4 GHz the E plane pattern shows ripple like behavior. The overlay enhances the oscillatory behavior especially in the -30^0 to 90^0 range. The H plane pattern shows lower R.P. The overlay doesn't change the situation much.

The consolidated data of the half power lobe width of all the radiation pattern is tabulated in table 3.5.

Table 3.5: Data of lobe width.

		Freq	$\Delta\theta_E$ (Deg)			$\Delta\theta_H$ (Deg)		
		GHz	W.O.	S1	S2	W.O.	S1	S2
P		9.2	14.7	14.7	14.7	47.05	44.11	52.94
A	L.S.F	8.1	29.41	76.47	73.52	79.41	82.35	79.41
T		8.65	94.11	88.23	82.35	100.00	94.11	94.11
C	S.S.F.	8.1	85.29	61.76	70.58	94.11	76.47	79.41
H		9.2	_	20.58	11.76	88.23	50.00	41.17
1	D.F.	8.1	41.17	29.41	32.35	94.11	79.41	70.58
P		10.4	23.52	41.17	55.88	52.94	50	50.00
A	L.S.F.	9.2	25.29	35.29	44.11	91.17	73.52	70.58
T		8.2	55.88	52.94	55.88	58.82	88.23	88.23
C	S.S.F.	8.3	50	58.82	52.94	102.94	82.35	73.52
H		9.4	29.41	52.94	55.88	58.82	50	44.11
2	D.F.	8.3	47.05	35.29	20.58	111.76	44.11	61.76

The semi theoretical gain calculations can be done from lobe width product formula reported by Lee at al [90].

$$\text{Gain (dB)} = 10 \log \left\{ \frac{26000}{\theta_E \times \theta_H} \right\}$$

Where θ_E and θ_H are the 3 dB down (half power) lobe widths for E and H plane radiation patterns respectively.

This formula gives the approximate directivity for antenna with single lobe patterns, as it is dependent on radiation pattern (without consideration of feed point and other losses).

Table 3.6 gives data of directivity gain of the EMC antenna studied. From table 3.6 it is seen that the overlay increases the directivity gain considerably for diagonally fed antenna.

Table 3.6 Data of directive gain

			Directivity Gain dB		
		Freq (GHz)	W.O.	S1	S2
P		9.2	15.75	16.03	15.23
A	LSF	8.1	11.13	6.16	6.48
T		8.65	4.41	4.95	5.25
C	SSF	8.1	5.10	7.4	6.66
H		9.2	___	14.03	17.29
1	DF	8.1	8.26	10.46	10.56
P		10.4	13.19	11.01	9.69
A	LSF	9.2	10.52	9.67	9.21
T		8.2	9.2	7.45	7.22
C	SSF	8.3	7.03	7.29	8.24
H		9.4	11.76	9.82	10.23
2	DF	8.3	6.94	12.82	13.10

3.3.3 Polarization measurements.

To get polarization plots microstrip patch antenna was rotated in the plane of the patch (XY plane) through 360^0 with axis of rotation along direction of propagation of the signal (Z axis). The power radiated is recorded for particular frequency with angle difference of 10^0. The relative power is plotted with respect to angle, which gives polarization plots.

The polarization plots Figure 3.23 indicated that at resonance for LSF (9.2 GHz), the radiated power is not symmetrical through 360^0 rotations. The antenna radiates in an end fired way with maxima at 180^0. The lobe at 180^0 is very small (of the order of 0.45 where as at 0^0 it is 1). Due to overlay the maxima 0^0 becomes less to 0.6 whereas at 180^0 it is still 0.45 for both S1 and S2. Only one thickness (2mm) of overlay was studied. At 8.1 GHz the antenna

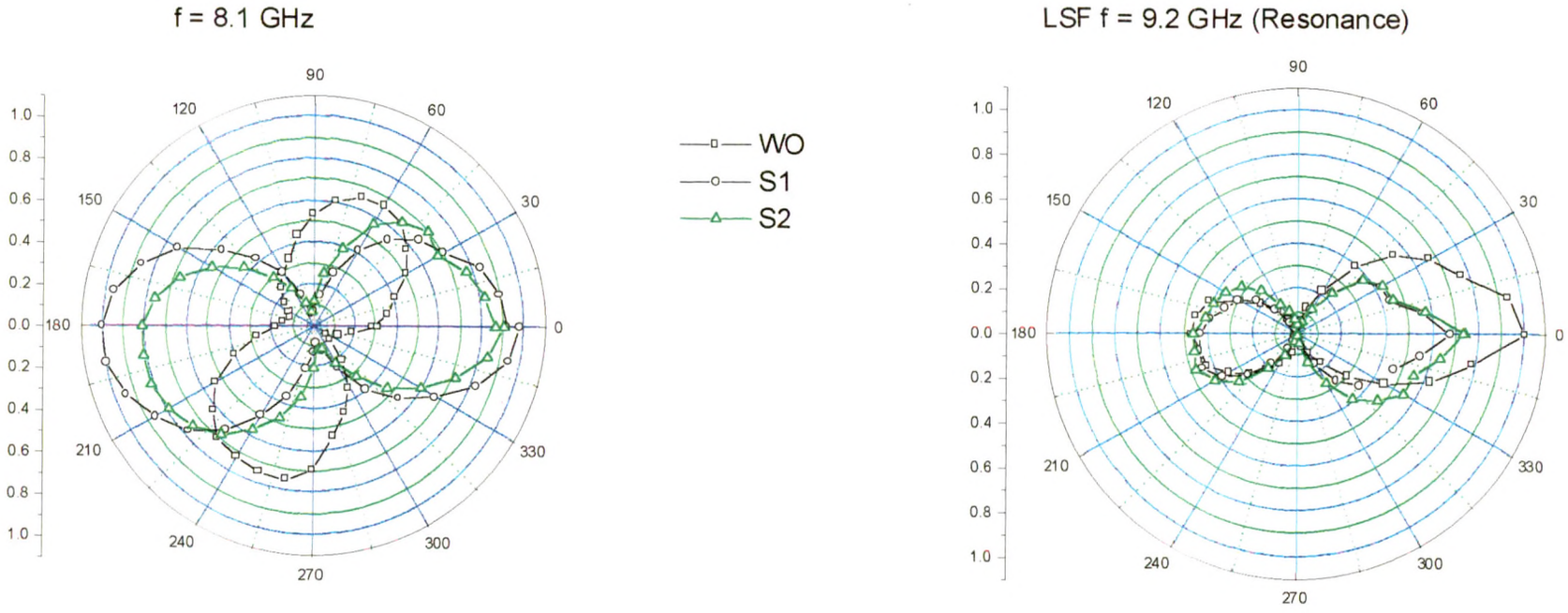

FIGURE 3.23 : Polar plot of Long Side Fed Patch 1 S1- MgFe2O4, S2- Mg0.4Mn0.5Zn0.1Al0.8Fe1.2O4

without overlay has maxima at 60^0 and 250^0 with a value of 0.55. Due to overlay of both S1 and S2 the maxima again comes back to 0^0 and 180^0 with a 0.8 value.

For the case of SSF, (Figure 3.24) at 8.1 GHz the antenna without overlay has maxima at 15^0 and broad maxima between 65^0-20^0. Due to overlay of S1 there is decrease in radiation at all angles whereas due to S2 there is increase in relative power. At 8.5 GHz the antenna without overlay shows maxima in the fourth quadrant at 345^0 and second quadrant. Here also due to S1 the relative power decreases and due to S2 it increases.

Figure 3.25 depicts the polarization plots for diagonally fed antenna. At 8.1 GHz the radiation maxima is approximately 45^0 and 230^0 with a value 0.9 and 0.6 respectively. Due to overlay of S1 the maxima has shifted between 50^0-60^0. In third quadrant, the radiated power has increased due to overlay. At 8.4 GHz, the angular direction has shifted to approximately 50^0 and 240^0 without overlay and due to overlay of S1 the maxima shifts to 70^0 and 250^0. The pattern has become very asymmetric with angular variation. Due to S2 overlay the radiated output increases without change in angle.

At 9.2 GHz the pattern has further rotated to give a maxima at approximately 90^0 and 300^0. Due to S1 overlay a further shift to 110^0 and 315^0 is observed with the radiated power becoming considerably higher in the fourth quadrant. Due to S2 overlay there is an indication of double maxima at 80^0 and 110^0.

These observations indicate the possibility of changing polarization properties of the patch antenna by means of either changing feeding position or use of ferrite overlay.

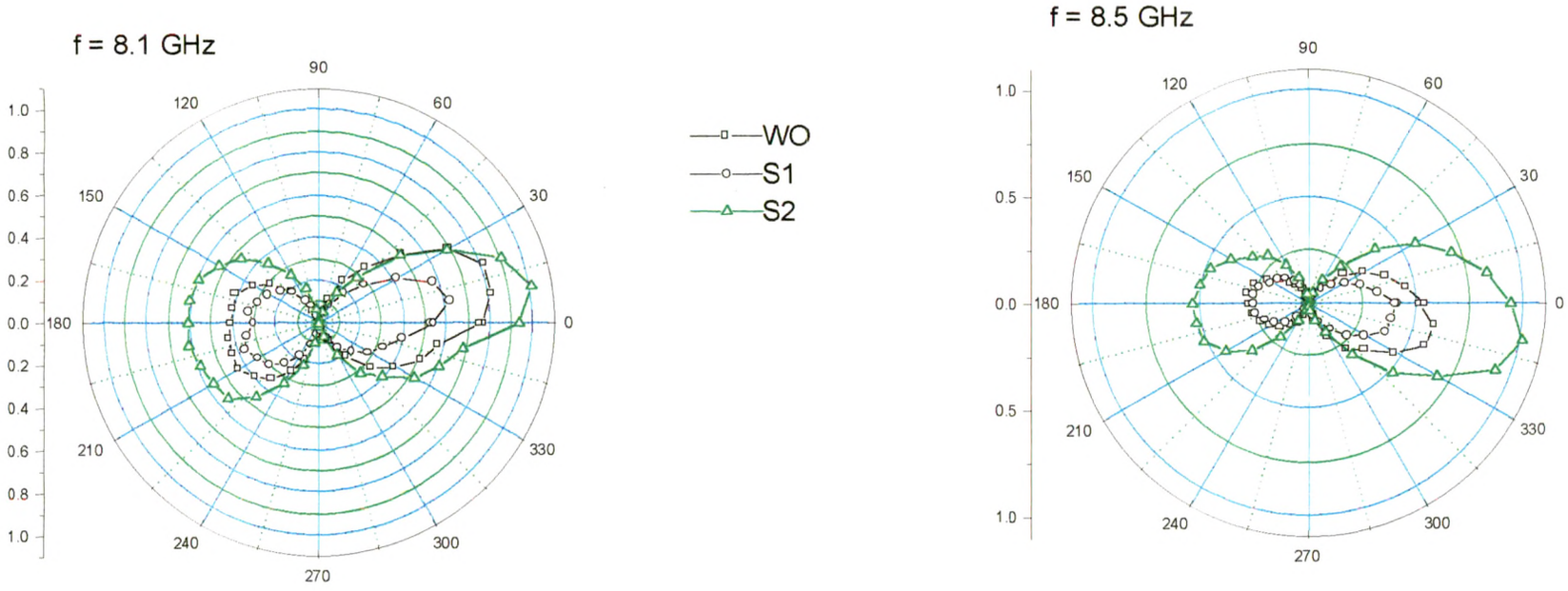

FIGURE 3.24 : Polar plot of Short Side Fed Patch 1 S1- MgFe2O4, S2- Mg0.4Mn0.5Zn0.1Al0.8Fe1.2O4

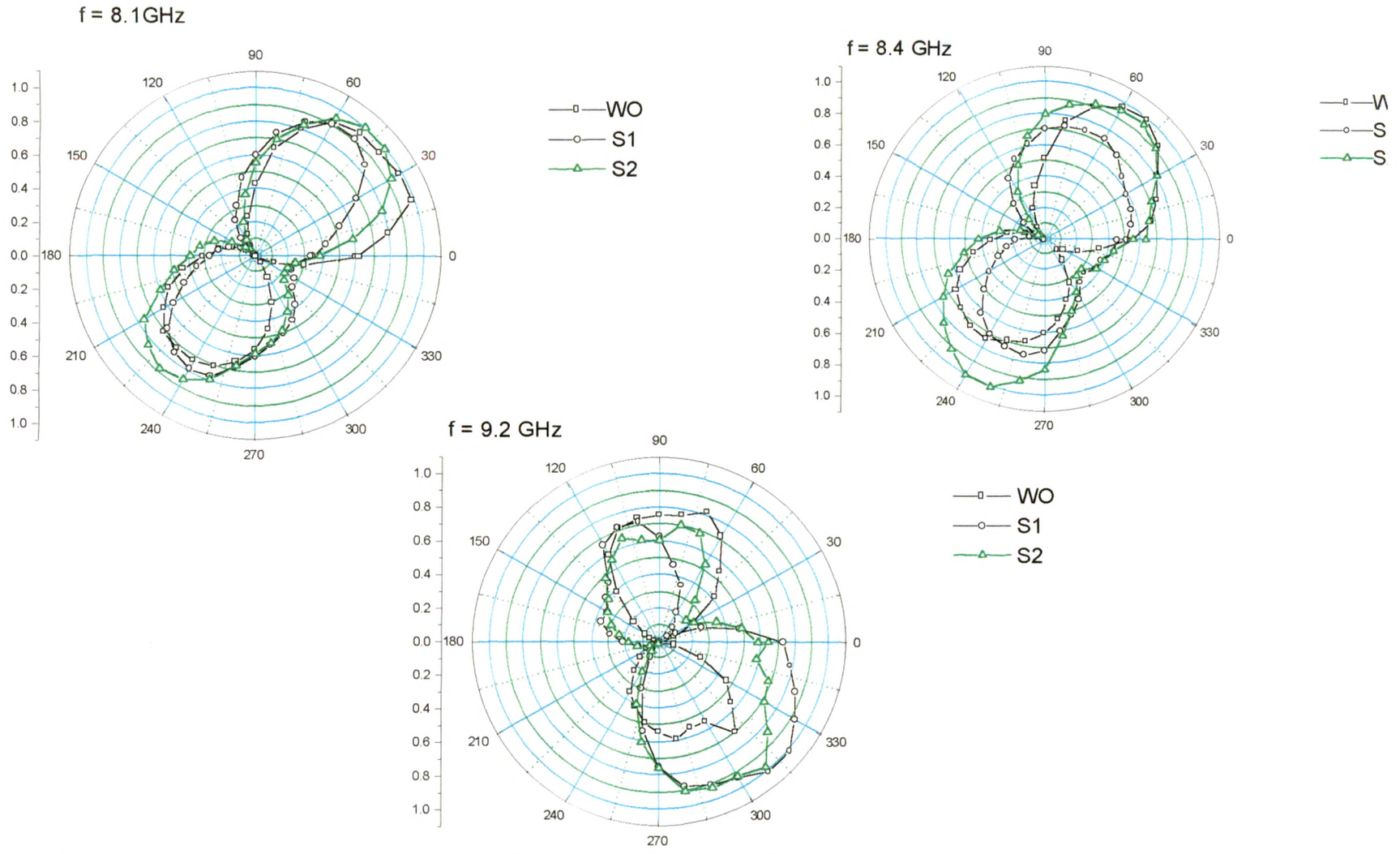

FIGURE 3.25 : Polar plot of Diagonally Fed Patch 1 S1- $MgFe_2O_4$, S2- $Mg_{0.4}Mn_{0.5}Zn_{0.1}Al_{0.8}Fe_{1.2}O_4$